ORIGINAL ARTICLE

The polyphenol EGCG directly targets intracellular amyloid-β aggregates and promotes their lysosomal degradation

Christopher Secker[1,2] | Angelika Y. Motzny[3] | Simona Kostova[1] | Alexander Buntru[1,4] | Lucas Helmecke[3] | Laura Reus[3] | Robert Steinfort[3] | Lydia Brusendorf[1] | Annett Boeddrich[1] | Nancy Neuendorf[1] | Lisa Diez[1] | Peter Schmieder[5] | Aline Schulz[1] | Constantin Czekelius[3] | Erich E. Wanker[1]

[1]Neuroproteomics, Max Delbrück Center for Molecular Medicine, Berlin, Germany

[2]Department of Neurology, Charité Universitätsmedizin Berlin, Berlin, Germany

[3]Institute for Organic Chemistry and Macromolecular Chemistry, Universität Düsseldorf, Düsseldorf, Germany

[4]Evotec SE, Hamburg, Germany

[5]Leibniz-Forschungsinstitut für Molekulare Pharmakologie (FMP), Berlin, Germany

Correspondence
Erich E. Wanker, Neuroproteomics, Max Delbrück Center for Molecular Medicine, 13125 Berlin, Germany.
Email: ewanker@mdc-berlin.de

Constantin Czekelius, Institute for Organic Chemistry and Macromolecular Chemistry, Universität Düsseldorf, 40225 Düsseldorf, Germany.
Email: constantin.czekelius@hhu.de

Funding information
Berlin Institute of Health, Grant/Award Number: 1.1.2.a.3; Bundesministerium für Bildung und Forschung; European Commission, Grant/Award Number: 01W1301

Abstract

The accumulation of amyloidogenic protein aggregates in neurons is a pathogenic hallmark of a large number of neurodegenerative diseases including Alzheimer's disease (AD). Small molecules targeting such structures and promoting their degradation may have therapeutic potential for the treatment of AD. Here, we searched for natural chemical compounds that decrease the abundance of stable, proteotoxic β-sheet-rich amyloid-β (Aβ) aggregates in cells. We found that the polyphenol (−)-epigallocatechin gallate (EGCG) functions as a potent chemical aggregate degrader in SH-EP cells. We further demonstrate that a novel, fluorescently labeled EGCG derivative (EGC-dihydroxybenzoate (DHB)-Rhodamine) also shows cellular activity. It directly targets intracellular Aβ42 aggregates and competes with EGCG for Aβ42 aggregate binding in vitro. Mechanistic investigations indicated a lysosomal accumulation of Aβ42 aggregates in SH-EP cells and showed that lysosomal cathepsin activity is critical for efficient EGCG-mediated aggregate clearance. In fact, EGCG treatment leads to an increased abundance of active cathepsin B isoforms and increased enzymatic activity in our SH-EP cell model. Our findings suggest that intracellular Aβ42 aggregates are cleared through the endo-lysosomal system. We show that EGCG directly targets intracellular Aβ42 aggregates and facilitates their lysosomal degradation. Small molecules, which bind to protein aggregates and increase their lysosomal degradation could have therapeutic potential for the treatment of amyloid diseases.

1 | INTRODUCTION

The accumulation of amyloidogenic protein aggregates in patient brains is a pathological hallmark of a large number of neurodegenerative disorders, including very common diseases like Alzheimer's disease (AD) or Parkinson's disease (PD), but also relatively rare genetic diseases like Huntington's disease (HD; Chiti & Dobson, 2017). Amyloid aggregates with a typical cross-β structure (Kollmer et al., 2019) are very stable, ordered protein assemblies, which are deposited both inside and outside of neuronal cells (Oddo et al., 2006). They generally consist of proteins that are specific to each disease, such as amyloid-β (Aβ) in AD, α-synuclein in PD, or huntingtin in HD (Pieri et al., 2012; Tipping et al., 2015) and may drive pathogenesis by a toxic gain of function mechanism (Engel et al., 2008; Kim et al., 2016; Nicoll et al., 2013; Volpicelli-Daley et al., 2011).

AD is characterized by the deposition of Aβ peptides in large extracellular amyloid plaques (Thal et al., 2015). These extracellular structures are found in patients with familial, early-onset AD as well as in sporadic cases (Castellani et al., 2006), suggesting that their formation and growth over time play a critical role in pathogenesis. However, various studies indicate that stable, β-sheet-rich Aβ aggregates are also formed in neurons and glia cells in AD brains, indicating that besides extracellular also intracellular structures are involved in disease development (Foley et al., 2020; Huang et al., 2020; LaFerla et al., 2007; Ripoli et al., 2014; Takahashi et al., 2017). This is also supported by observations in AD model systems, demonstrating that the formation of intracellular Aβ aggregates precedes the accumulation of extracellular deposits (Gyure et al., 2001; Wirths et al., 2001) and that these structures can promote tau aggregation (Götz et al., 2001; He et al., 2018; Zempel et al., 2010), which is associated with neuronal dysfunction and progression of disease (Zhou et al., 2017). Additionally, recent studies indicate that preformed, fibrillar Aβ structures are very efficiently taken up into mammalian cells (Yeh et al., 2016) supporting the view that self-propagating protein templates, often termed as "seeds" can enter cells and thereby have the potency to convert intracellular Aβ molecules from a soluble into an aggregated state (Sowade & Jahn, 2017).

Several lines of experimental evidence indicate that small toxic oligomeric Aβ assemblies play a critical role in neurodegeneration in AD (Benilova et al., 2012). These structures are efficiently taken up into hippocampal neurons and were recently shown to induce toxicity more efficiently than mature amyloid fibrils (Vadukul et al., 2020), suggesting that they have unique properties that make them neurotoxic. Currently, the molecular mechanisms by which prefibrillar and/or fibrillar (Stroud et al., 2012) oligomeric Aβ42 species cause cognitive impairment or neurodegeneration

are largely unclear. However, it may well be that insufficient cellular clearance of amyloid structures in the endosomal-lysosomal network (Knopman et al., 2021; Marshall et al., 2020) may play a critical role in disease. This is also supported by recent investigations in different AD transgenic mouse models, indicating that the formation of abnormal lysosomal structures that contain fibrillar Aβ aggregates in neurons likely is an important early event in pathogenesis (Lee et al., 2022).

Using cell-free assays, various types of chemical compounds have been previously identified that target Aβ peptides and interfere with their self-assembly into β-sheet-rich, fibrillar aggregates (Velander et al., 2017). Furthermore, compounds that directly bind to fibrillar amyloid aggregates and remodel or stabilize these structures in vitro have been described (Ehrnhoefer et al., 2008; Haney et al., 2017; Ladiwala et al., 2010; Sharoar et al., 2012). Whether small molecules can be identified, however, that function as chemical aggregate degraders (CADs) in cells and promote the clearance of preformed β-sheet-rich aggregate assemblies is currently unclear. Chemical compounds (also known as proteolysis-targeting chimeras, "PROTACs") that promote the degradation of soluble proteins by linking the target protein to the ubiquitin-proteasome system (UPS) have been reported (Bondeson et al., 2015; Schneekloth et al., 2008). However, high molecular weight amyloidogenic protein aggregates in cells are normally not degraded by the UPS but rather are digested by autophagic pathways, which involves their sequestration into autophagosomes and lysosomes (Leeman et al., 2018; Lu, den Brave, et al., 2017).

Here, we present the establishment of a cell-based assay that can be applied to search for CADs that promote the degradation of stable, fluorescently labeled Aβ42 aggregates in neuroblastoma cells. We screened a focused library of potential amyloid-binding polyphenolic compounds (Ehrnhoefer et al., 2006; Gazova et al., 2013; Ono et al., 2003) and identified the compound (−)-epigallocatechin gallate (EGCG) as a potent CAD. We found that EGCG directly targets stable, β-sheet-rich Aβ42 aggregates, which are rapidly internalized from the extracellular space into mammalian cells, and promotes their degradation in lysosomes. This result is also supported by mechanistic investigations in cells, indicating that EGCG increases the processing of preformed β-sheet-rich fibrillar Aβ42 aggregates by lysosomal cathepsins. The potential implications of our results for the development of CADs are discussed.

2 | METHODS

Institutional ethical approval was not required for this study. The study was not pre-registered. Custom-made materials used in this study can be shared upon reasonable request if available.

2.1 | Aβ (1–42) peptide stock solutions

Synthetic Aβ (1–42) (Aβ42) peptides produced via solid-state peptide synthesis (BACHEM, RRID:SCR_013558) were dissolved in 1,1,1,3,3,3-hexafluoro-2-propanol (HFIP, Sigma-Aldrich, RRID:SCR_008988) for 72h, sonicated three times for 30min, aliquoted and lyophilized with a SpeedVac Plus (Savant). Monomeric Aβ solutions (200μM) were prepared from HFIP-treated peptides by dissolution in 10mM NaOH, sonication for 5min, and were diluted in low salt buffer (2mM KH_2PO_4, 8mM K_2HPO_4, 10mM NaCl) to desired concentrations. Lyophilization and handling of Aβ42 solutions were performed in 1.5mL Protein LoBind tubes (Eppendorf) to minimize the binding of peptides to plastic surfaces.

2.2 | Generation and fluorescent labeling of Aβ42 aggregates

Aβ42 aggregates were prepared from 20μM peptide stock solutions by incubation in low salt buffer (2mM KH_2PO_4, 8mM K_2HPO_4, 10mM NaCl) at 37°C for 18h under constant agitation (300rpm) in a Thermomixer (Eppendorf). For fluorescent labeling of Aβ42 aggregates, 20μM Aβ42 peptide stock solutions diluted in low salt buffer (2mM KH_2PO_4, 8mM K_2HPO_4, 10mM NaCl) were mixed with 5% Aβ42 peptides, which have been N-terminally labeled with the fluorophore 5-carboxytetra-methylrhodamine (TAMRA; AS-60476, AnaSpec, RRID:SCR_002114) or HiLyte 488 Fluor (AS-60479, AnaSpec, RRID:SCR_002114) in solid-state peptide synthesis. Then, mixed Aβ42 peptide solutions were aggregated at 37°C for 18h under constant agitation (300rpm). For cellular uptake experiments, fluorescently labeled co-aggregates ([TAMRA]Aβ42/Aβ42, [HiLyte]Aβ42/Aβ42) or unlabeled Aβ42 aggregation products were additionally tip sonicated (Ultrasonicator 450, Branson) at the lowest intensity for 1min.

2.3 | 19F-nuclear magnetic resonance-spectroscopy

The first two samples for nuclear magnetic resonance (NMR)-spectroscopy were prepared by dissolving HFIP in 600μL of a buffer consisting of 90% H_2O and 10% D_2O to yield concentrations of 10 or 1mM (samples 1 and 2, Figure S1). A third sample was prepared by using a solution of 50μM Aβ42 in a buffer consisting of 90% H_2O and 10% D_2O, no HFIP was added (sample 3, Figure S1). The samples were transferred into 5mm NMR sample tubes. NMR spectra were recorded at 300K at 600 MHz (1H frequency) on a Bruker AV-III spectrometer (Bruker Biospin) using a 5mm broadband probe ("BBFO") equipped with one-axis self-shielded gradients. The software used to control the spectrometer was topspin 3.5 pl6. The temperature had been calibrated using d4-methanol and the formula of Findeisen. One-dimensional 19F-spectra were recorded using inverse gated decoupling, a spectral

width of 50kHz, and an acquisition time of 1.31s. A relaxation delay of 20s was used to allow for full relaxation. Data were processed using topspin3.5pl6, and an exponential line-broadening of 5Hz was used. The spectra were referenced externally according to the International Union of Pure and Applied Chemistry relative to trifluoroacetic acid.

2.4 | Atomic force microscopy

Sheet mica (Nanoworld) was glued to conventional microscope slides and 20μL sample solution was adsorbed for 15min onto the freshly cleaved mica, washed with filtered, deionized water (5×40μL), and dried overnight. As a control, aggregation buffer was added to the mica slide. Sample images were recorded with a digital multimode NanoWizard II atomic force microscope (jpk instruments) using a cantilever with a resonance frequency f0 of 75kHz (Bruker AFM Probes) in intermittent contact mode.

2.5 | Thioflavin T-based quantification of aggregates

Aβ42 aggregates or [TAMRA]Aβ42/Aβ42 co-aggregates were transferred to black 384-well microtiter plates (353952, BD Falcon) and incubated for 20min with equimolar thioflavin T (ThT, Sigma-Aldrich, RRID:SCR_008988) diluted in aggregation buffer. ThT fluorescence (Ex/Em 420/485nm) was quantified using a fluorescence microplate reader (Tecan M200 Multi-mode Microplate Reader, RRID:SCR_020543).

2.6 | Quantification of SDS- and NP40-stable Aβ42 aggregates with filter retardation assays

For analysis of insoluble aggregates in denaturing filter retardation assays (dFRAs, detection of sodium dodecyl sulfate (SDS)-stable aggregates), samples were monitored by adding them to an equal volume of SDS (final concentration: 2%) and 100mM dithiothreitol (DTT) and boiling at 98°C for 5min. For analysis of Aβ42 aggregates under non-denaturing conditions with a native filter retardation assay (nFRA, detection of native aggregates), samples were mixed with an equal volume of nonyl phenoxypolyethoxylethanol (NP40) solution (final concentration: 0.1%). Then, nFRA or dFRA samples were filtered through a cellulose acetate membrane with 0.2μm pores (OE66, Schleicher and Schuell). Membranes were blocked in TBS containing 3% skim milk. Aggregates retained on the filter membrane were either detected using the Aβ-specific antibodies 6E10 (1:2000, BioLegend, RRID:SCR_001134) or 4G8 (1:2000, BioLegend, RRID:SCR_001134) and an anti-mouse secondary antibody conjugated to HRP for detection of chemiluminescence after addition of horseradish peroxidase (HRP) substrate or, in case of [TAMRA]Aβ42/Aβ42 co-aggregates, via detection of the rhodamine

fluorescence signal intensities on the filter membrane by exciting with a green light source (520 nm) and detecting with a long-pass emission filter (>575 nm) with a LAS-3000 Imaging System (Fujifilm). Signal intensities were quantified from technical triplicates after background subtraction using Aida Image Analyzer Software (Elysia-raytest).

2.7 | Fluorescence polarization-based Aβ42 aggregation assay

N-terminally 5-carboxyfluorescein (FAM)-labeled Aβ42 peptides (AS-23525-05, AnaSpec, RRID:SCR_002114) were dissolved in 1 mM NaOH to 50 μM and stored as a stock solution at −20 °C (Aβ42-FAM tracer). In Aβ42 aggregate reactions 0.05 μM Aβ42-FAM tracer was combined with 10 μM unlabeled Aβ42 peptides in low salt buffer (2 mM KH_2PO_4, 8 mM K_2HPO_4, 10 mM NaCl). For seeded aggregation reactions, tip sonicated (5 s, Ultrasonicator 450, Branson; at lowest intensity) 80 nM (monomer equivalent) preformed Aβ42 aggregates were added as seeds. The aggregation mixtures were replenished with low salt buffer to a total volume of 40 μL/well. Fluorescence polarization (FP) was measured every 15 min at 37 °C in a fluorescence microplate reader with a polarization module (Tecan M1000/M1000 PRO Multi-mode Microplate Reader) at an excitation wavelength of 470 ± 5 nm and an emission wavelength of 528 ± 20 nm in 384 well plates (781 906, Greiner Bio-One) with 5 s shaking before each read. Mean values are from four technical replicates. Polarization values are calculated as dimensionless millipolarization units (mP) using the plate reader software i-control (Tecan Life Sciences, RRID:SCR_016771).

2.8 | Neuroblastoma cell culture and cell treatment with ^{TAMRA}Aβ42/Aβ42 co-aggregates

Human neuroblastoma SH-EP cells (RRID:CVCL_0524) were cultured in DMEM (Gibco) containing 10% fetal bovine serum (FBS), 5% glucose, 100 units/mL penicillin and streptomycin, respectively. Incubation was carried out at 37 °C with 5% (v/v) CO_2 and cells were used until passage number 20. For aggregate internalization, cells were treated with 600 nM or 1 μM ^{TAMRA}Aβ42/Aβ42 co-aggregates for 2, 4, 6, or 8 h via direct infusion into the cell culture medium. Aggregate incubation was stopped by washing cells with PBS, exchange of culture medium, and trypsinization.

2.9 | Automated fluorescence microscopy and determination of cellular Aβ42 aggregate loads

Cells were treated with ^{TAMRA}Aβ42/Aβ42 co-aggregates or ^{HiLyte}Aβ42/Aβ42 co-aggregates as described above for the indicated timeframes. To ensure the removal of surface-bound aggregates, the medium was aspirated, cells were washed with PBS, trypsinized,

centrifuged at 150×g for 3 min, and collected in fresh medium. Then, cells were seeded into 96-well cell culture plates (353 219, BD Falcon). After adhesion, cells were fixed in 2% paraformaldehyde (PFA) for 20 min at room temperature (RT), followed by nuclei staining with Hoechst 33342 (1:2500), and then washed twice with PBS. Fluorescence microscopy was performed in a Cellomics ArrayScan High-Content System (Thermo Fisher Scientific, RRID:SCR_008452) using an objective with 20-fold magnification. Of each well, a minimum of five to a maximum of nine images were recorded and analyzed; each image contained ~20 individual cells. After image acquisition, automated data analysis was performed using the ArrayScan VTI software (Thermo Fisher Scientific, RRID:SCR_008452). For quantification, individual cells were identified from Hoechst signals (Ex/Em 350/461 nm) and mean circular TAMRA (Ex/Em 555/580 nm) or HiLyte 488 (502/527 nm) spot count or total TAMRA spot area per cell was measured and calculated from technical triplicates. Aggregate load per cell was quantified by dividing the total TAMRA fluorescent area per image by the cell count per image.

2.10 | Enrichment of lysosomes from SH-EP cells

For the preparation of samples, SH-EP cells (~36 × 10^6 cells) were treated with 1 μM preformed Aβ42 aggregates or buffer as control. Cells were washed, trypsinized, and harvested. Then, lysosomes were enriched using the Minute Lysosome Isolation Kit (Cat. No. LY-034, Invent Biotechnologies) according to the manufacturer's protocol. In brief, cells were washed with cold PBS, resuspended in buffer A (undisclosed components), and incubated on ice for 5–10 min. The cell suspension was then vortexed for 30 s and 50 μL of the lysate was saved as total protein. The remaining lysate is transferred to the filter cartridge, inverted a few times, and centrifuged with 16 000×g for 30 s. The pellet was resuspended by vortexing for 10 s and was centrifuged with 2000×g for 3 min. The supernatant was transferred to a fresh tube and centrifuged at 4 °C with 11 000×g for 15 min. 400 μL of the supernatant was transferred to a fresh tube and centrifuged at 4 °C with 16 000×g for 30 min. The supernatant was discarded and the pellet was resuspended in 100 μL of buffer A and centrifuged with 2 000×g for 4 min. The supernatant was carefully transferred to a fresh tube and 50 μL buffer B (undisclosed components) was added, mixed, and incubated for 30 min on ice. The supernatant was removed completely and the pellet was resuspended in 30 μL PBS (lysosomal fraction). Protein concentration of total and lysosomal fractions was determined using a bicinchoninic acid protein assay kit (Pierce BCA Protein Assay Kit, Thermo Fisher Scientific, RRID:SCR_008452), and 10 μg of each sample was analyzed by polyacrylamide gel electrophoresis and western blotting as described above. Anti-LAMP1 (1:1000, ab62562, abcam, RRID:AB_2134489), anti-flotilin-1 (1:1000, #3253, Cell Signaling, RRID:AB_210673) and 6E10 anti-Aβ (1:1000, 803 002, BioLegend, RRID:AB_2564654) primary antibodies and anti-rabbit or anti-mouse HRP-coupled secondary antibodies were used for detection.

2.11 | Screening of polyphenol compound library

A compound library containing 20 polyphenol molecules was utilized for the focused screen. Compounds were purchased from Sigma-Aldrich (RRID:SCR_008988). All compounds were at analytical grade (>95% purity or higher) and dissolved in DMSO at 20 mM and stored at −20 °C. To test their cellular Aβ42 degradation promoting effect, cells previously treated for 6 h with ^{TAMRA}Aβ42/Aβ42 co-aggregates as described above were washed with PBS, trypsinized, and collected accordingly. Then, ^{TAMRA}Aβ42/Aβ42 co-aggregates harboring cells were seeded onto 10 μM compound dilutions or DMSO only as control and incubated for an additional 20 h. Automated fluorescence microscopy and data analysis to determine cellular Aβ42 aggregate load was performed as described above. To check for false-positive hits, compounds with significant reduction of TAMRA spot counts per cell were tested for their effect on the TAMRA fluorophore alone. Therefore, 1 μM TAMRA (5-TAMRA, C6121, Invitrogen) and 1 μM compound were incubated together in 40 μL PBS for 15 min at RT in a 384-well plate (781 906, Greiner Bio-One). PBS only or DMSO were used as buffer controls. TAMRA fluorescence intensity was quantified in a TECAN M1000 Microplate Reader (Ex/Em 550/580 nm).

2.12 | Immunocytochemistry

SH-EP cells were washed with PBS before fixation with 2% PFA for 15 min at RT, Hoechst 33342 staining (1:2500) followed by permeabilization with 0.1% Triton in PBS and blocking with 1% bovine serum albumin (BSA) in PBS containing 0.05% Triton-X100 (PBS-T). For immunofluorescence staining, cells were incubated with primary antibodies (1:1000 anti-Aβ/APP, 6E10, BioLegend, RRID:SCR_001134; 1:500 anti-LAMP2, H4B4, Invitrogen, RRID:AB_2662613; 1:500 anti-α-tubulin, T6199, RRID:AB_477583) overnight at 4 °C or 2 h at 37 °C, subsequently with secondary antibodies for 1 h at RT and washed with PBS before visualization. For staining of β-sheet-rich intracellular aggregates, cells were treated with 10 μg/mL of the amyloid-binding compound Thioflavin S (ThS) for 10 min at RT and then washed with PBS.

2.13 | Confocal microscopy

For confocal microscopy, 9.0×10^4 SH-EP cells per well were seeded on fibronectin and poly-D-lysine-coated (1:100) coverslips in 24-well cell culture plates (662 160, Greiner Bio-One). Fixation and immunocytochemistry were performed as described above. Coverslips were then transferred to conventional microscope slides using a fluorescence mounting medium (Dako S3032, Agilent Technologies) before image acquisition with a Leica TCS SP5 confocal microscope was performed (at Advanced Light Microscopy Facility, MDC). Cells were identified from Hoechst fluorescence signals (Ex/Em 353/483 nm); TAMRA, FITC, HiLyte 488, and ThS fluorescent

images were acquired at excitation wavelengths of Ex/Em 555/580, 490/525, 497/526, and 384/429 nm, respectively. Co-localization analysis of TAMRA with FITC, TAMRA with HiLyte 488, or TAMRA with ThS fluorescent puncta was performed using the Fiji Software (https://imagej.net/Fiji).

2.14 | Preparation of cell lysates for biochemical analysis and compound validation

Cell lysates for biochemical analysis were prepared as follows: 2.2×10^6 SH-EP cells were seeded into T25 cell culture flasks. After adhesion overnight, cells were treated with ^{TAMRA}Aβ42/Aβ42 co-aggregates directly infused into the cell culture medium as described above for indicated timeframes. Then, cells were washed with PBS, trypsinized, and collected in a fresh medium. For compound validation experiments, cells were incubated with aggregates for 6 h, washed and trypsinized, and then seeded onto wells pre-filled with EGCG or DMSO as control. After incubation of 20 h with DMSO, 10, 20, or 30 μM EGCG, cells were collected in fresh medium and centrifuged for 3 min at 150×g in an Allegra X-12 centrifuge (Beckman Coulter). After an additional washing step in PBS, cell pellets were lysed with 150 μL cell lysis buffer (50 mM Tris pH 8, 1 mM EDTA, 100 mM NaCl, 5 mM MgCl$_2$, 1% NP40, 1 mM PMSF, 1× protease inhibitor cocktail (cOmplete, Roche), 1:1000 Benzonase [Merck Millipore]) for 30 min at 4°C. Protein concentrations of cell lysates were determined using a bicinchoninic acid protein assay kit (Pierce BCA Protein Assay Kit, Thermo Fisher Scientific, RRID:SCR_008452) and were subsequently stored at −80 °C in Protein LoBind tubes (Eppendorf).

2.15 | Polyacrylamide gel electrophoresis and western blotting

For analysis of samples by polyacrylamide gel electrophoresis (PAGE), 20 μg cell lysates were added to 1× sample buffer (SB, NuPAGE LDS Sample Buffer +100 mM DTT, Thermo Fisher Scientific, RRID:SCR_008452) before being boiled for 5 min at 95 °C in Protein LoBind tubes in a Thermomixer (Eppendorf). Then, samples were loaded into gel pockets of 1 mm Bis-Tris 4%–12% polyacrylamide gels (NuPAGE, Invitrogen) along with a pre-stained protein standard (SeeBlue Plus2, Thermo Fisher Scientific, RRID:SCR_008452). After electrophoresis for 35 min at 200 V with 1× MES SDS running buffer (NuPAGE, Invitrogen), separated protein from cell lysates was wetly blotted onto a nitrocellulose membrane (Protran BA85 0.45 μm, Amersham) with transfer buffer (25 mM Tris, 192 mM glycine, 10% methanol). Membranes were blocked with 3% milk powder (Carl Roth) in PBS-T for 1 h at RT. Then, membranes were incubated overnight at 4 °C in blocking solution with primary antibodies (Aβ antibodies: 6E10, 1:1000; 4G8, 1:1000, BioLegend, RRID:SCR_001134; cathepsin B: ab58802, 0.25 μg/mL, Abcam, RRID:SCR_012931; tubulin: ab6046, 1:1000, Abcam, RRID:SCR_012931), followed by washing in PBS-T and subsequent incubation with HRP conjugated

secondary antibodies for an additional hour at RT. For detection, HRP substrate (Pierce ECL Western Blotting Substrate, Thermo Fisher Scientific, RRID:SCR_008452) was added and chemiluminescence was measured with a LAS-3000 Imaging System (Fujifilm).

2.16 | Live/dead toxicity assay

SH-EP cells were seeded on day 0 in 6-well cell culture plates (657 160, Greiner Bio-One) at an initial density of 5×10^5 cells per well. The next day (day 1), cells were treated with $1 \mu M$ Aβ42 aggregates (prepared as described above) or buffer as control. At the same timepoint, cells were treated with 10, 20, 50, or 100 μM EGCG. After incubation for 20 h (day 2), cells were washed, harvested in PBS, and stained with propidium iodide and calcein-AM according to the manufacturer's protocol (Live/Dead™ Viability/Cytotoxicity Kit, Invitrogen). For the generation of dead cells as a positive control, an untreated well was incubated in the presence of 0.05% Triton-X100 for 15 min prior to staining. For a control cell population containing live and dead cells, untreated and Triton-X100-treated cells were mixed at a ratio of 1:1. Cells were analyzed on an Aria III cell sorter (BD Biosciences) by first gating for both live and dead cells using forward and sideward scatters. Propidium iodide-permeable cells were identified by excitation with a yellow/green laser and a 610/620 nm bandpass filter, and calcein-positive cells were identified by excitation with a blue laser and a 530/530 nm bandpass filter. The gate for quantification of dead cells was selected using the Triton-X100 and a mixed sample containing both untreated and Triton-X100-treated cells.

2.17 | MTT assay

For analysis of Aβ42-induced toxicity on neuroblastoma cells, SH-EP cells were cultured as described above and seeded at an initial density of 2.0×10^4 cells per well into 96-well cell culture plates (650 180, Greiner Bio-One). Neuroblastoma cells were then treated with $1 \mu M$ preformed [TAMRA]Aβ42/Aβ42 co-aggregates or aggregation buffer as control. Cells were treated with indicated EGCG concentrations and further incubated for 20 h. To evaluate Aβ42-induced toxicity, MTT (3-(4,5-dimethylthiazol-2-yl)-2,5-diphenyltetrazolium bromide) reagent (M6494, Thermo Fisher Scientific, RRID:SCR_008452) was added to the cell culture medium and cells were incubated for additional 4 h at 37 °C. Finally, a stop solution was applied, cells were incubated for 1 h and absorbance was measured at 570 nm in a microplate reader (Tecan M200 Multi-mode Microplate Reader, RRID:SCR_020543).

2.18 | Cathepsin B activity in cellular lysates

SH-EP cells were treated with [TAMRA]Aβ42/Aβ42 co-aggregates as described above. Cells were then washed, trypsinized and 9×10^5 cells were replated onto 6-well cell culture plates (657 160, Greiner Bio-One). After 20 h of incubation with DMSO, 10 nM bafilomycin A1 (328 120 001,

Thermo Fisher Scientific, RRID:SCR_008452) or 5 μM CA074me (205 531, Sigma-Aldrich, RRID:SCR_008988) cells were washed with PBS, mechanically harvested and lysed using M2 lysis buffer (50 mM Tris, 150 mM NaCl, 50 mM NaF, 5 mM Na_3PO_4, 0.1 mM Na_3VO_4, 40 mM β-glycerol PO_4, 1 mM EDTA, 1 mM AEBSF, 0.1 mM PMSF) at 4°C for 1 h in Protein LoBind tubes (Eppendorf). The protein concentration of SH-EP cell lysates was determined using a bicinchoninic acid protein assay kit (Pierce BCA Protein Assay Kit, Thermo Fisher Scientific, RRID:SCR_008452). SH-EP cell lysates were diluted to 1 $\mu g/\mu l$ in cell-free system buffer (10 mM HEPES-NaOH, 2.5 mM KH_2PO_4, 2 mM NaCl, 2 mM $MgCl_2$, 0.5 mM EGTA, 5 mM pyruvate, 68 mM D-sucrose, 220 mM D-mannitol, 1 mM AEBFS, 0.1 mM PMSF, 1 mM DTT). Finally, 25 μg cell lysate was added to prediluted fluorescence quenching cathepsin B substrate Z-Arg-Arg 7-amido-4-methylcoumarin (Z-R-R-AMC, C5429, Sigma-Aldrich, RRID:SCR_008988) at a final concentration of 50 μM. After 1 h, substrate turnover was quantified by measuring AMC fluorescence intensity (Ex/Em 348/440 nm) in a 96-well quartz plate (730.009B-QG, Hellma Analytics) in a Tecan M1000 PRO Multi-mode Microplate Reader.

2.19 | Synthesis of rhodamine-labeled EGCG derivative

A detailed synthesis pathway is outlined in the scheme in Figure S5. The PEG-linker (#2) was prepared from triethylene glycol (#1) by ditosylation and stepwise nucleophilic substitution of the tosylate groups with sodium azide. The synthesis of azido-functionalized gallic acid started with orthoester protection of methyl gallate (#3) and alkylation of the remaining hydroxy group on orthoester-protected methyl gallate (#4) with tosylate (#2). Subsequent acidic orthoester cleavage led to the 1,2-diol, which upon dibenzylation and saponification furnished the desired PEG-linker (#5). cis-Chromanol was previously prepared according to the literature following a procedure by Krohn et al. (2009). Protected cis-chromanol (#6) was substituted by Steglich esterification with the azido-functionalized linker (#5) resulting in (#7) in 75% yield. The azido functionality of (#7) served as a handle for the click reaction with alkynyl-functionalized rhodamine (#8) giving the benzyl-protected coupling product. Final hydrogenolytic cleavage of the benzyl-protecting groups using Pearlman's catalyst afforded compound (#9) in 57% yield. For the generation of the rhodamine B-labeled control compound, the azido-functionalized, orthoester-protected methyl gallate (#4) was coupled with alkynyl-functionalized rhodamine (#8). The following deprotection by the use of pyridinium p-toluenesulfonate (PPTS) yielded compound (#10) missing the cis-chroman-3-ol moiety in 77% yield.

2.20 | Co-localization experiments with rhodamine-labeled EGCG derivative

SH-EP cells were treated with preformed [HiLyte]Aβ42/Aβ42 co-aggregates for ~6 h, washed, trypsinized, and re-plated on

coverslips as described above. After cell adhesion, wells were treated with 20 μM EGC-DHB-Rhodamine or DHMB-Rhodamine as a control for 3 h. Then, cells were fixed, stained with Hoechst, mounted, and subjected to confocal microscopy as described above. Hoechst signals (Ex/Em 350/461 nm), HiLyte 488 (502/527 nm) and Rhodamine B (Ex/Em) signals were recorded at their respective wavelength spectrum. Co-localization analysis of each selected region of interest (ROI) was performed using the RGB_Profiler plugin for ImageJ (https://imagej.nih.gov/ij/plugins/rgb-profiler.html). The correlation of HiLyte and rhodamine fluorescence intensities was analyzed using GraphPad Prism (RRID:SCR_002798) version 9.3.1.

2.21 | Competitive compound binding to Aβ42 aggregates

For compound binding assays, we first generated Aβ42 aggregates as described above (20 μM Aβ42 peptides in low salt buffer (2 mM KH_2PO_4, 8 mM K_2HPO_4, 10 mM NaCl) incubated at 37°C for 18 h under constant agitation at 300 rpm). Then, we used an in-house generated dot blotting device to immobilize preformed Aβ42 aggregates. We first equilibrated the nitrocellulose membrane (Whatman Protran BA85, 0.2 μm) with 100 μL low salt buffer, then applied 250 ng of preformed aggregates, and washed the immobilized aggregates again with 100 μL low salt buffer. Next, dotted aggregates were incubated for 15 min at RT with DMSO, 10 μM DHMB-RhB, or 10 μM EGC-DHB-RhB in the absence or presence of 10 or 20 μM EGCG or GC, respectively. Finally, the rhodamine B fluorescence of dots was measured from rhodamine B fluorescence intensity using an iBright Imaging System (Invitrogen). The intensity of each dot was quantified using the Fiji Software (https://imagej.net/Fiji).

2.22 | Statistical analyses and information on data reporting

Statistical analyses were performed as indicated in the respective figure legends. For the in vitro experiments conducted in this study, no normality assessment or blinding was performed. To estimate the sample size and to verify experimental planning for sufficient power, we conducted power analyses using the R package "pwr2" (Lu, Liu, et al., 2017) aiming for a medium ($d=0.5$) or large ($d\geq0.8$) effect size (Carson, 2012; Sullivan & Feinn, 2012), no sample calculation or blinding was performed. No test for outliers or outlier elimination was performed. For the comparison of data from three or more unmatched groups defined by one factor, one-way ANOVA with Dunnett's or Tukey's post hoc testing was performed. For the comparison of data from three or more unmatched groups defined by two factors, two-way ANOVA with Bonferroni's or Dunnett's post hoc testing was performed. All statistical analyses were performed using GraphPad Prism (RRID:SCR_002798) version 9.3.1. An overview of all statistical tests is provided in Table 1. No formal randomization procedures were applied to allocate treatments to the differential experimental groups of cultured cells. The human neuroblastoma cell line used in this study (SH-EP, RRID:CVCL_0524) is not listed as a commonly misidentified cell line by the International Cell Line Authentication Committee. No further authentication of the cell line was performed in the laboratory.

3 | RESULTS

3.1 | Generation and biochemical characterization of fluorescently labeled fibrillar TAMRA Aβ42/Aβ42 co-aggregates

We first established a procedure for the reproducible preparation of fluorescently labeled fibrillar Aβ42 aggregates for degradation studies in mammalian cells. We generated co-aggregates, which contain Aβ42 peptides labeled with the pH-insensitive fluorescent dye TAMRA (Shiba et al., 2017). Therefore, we incubated HFIP-monomerized Aβ42 peptides (20 μM) with TAMRA Aβ42 tracer peptides (5%) for 18 h at 37°C and analyzed the spontaneously formed TAMRA Aβ42/Aβ42 co-aggregates by atomic force microscopy (AFM). In control reactions, high molecular weight aggregates were also produced from Aβ42 monomers (20 μM) in the absence of tracer molecules. Aβ42 peptide solutions were also analyzed for their remaining HFIP content by NMR-spectroscopy. Residual HFIP was still detectable, however at a concentration of ~0.002% (v/v; Figure S1), which is ~1000-fold lower than the concentrations at which substantial effects on Aβ aggregation were previously reported (Nichols et al., 2005). Importantly, comparing unlabeled Aβ42 to TAMRA Aβ42/Aβ42 co-aggregates, we found that in both reactions amyloidogenic aggregates with a typical fibrillar morphology (Gremer et al., 2017; Schmidt et al., 2009) were produced (Figure S2A), indicating that the addition of low amounts of TAMRA Aβ42 tracer molecules does not significantly alter the fibril formation process.

To assess whether the generated fibrillar TAMRA Aβ42/Aβ42 co-aggregates are β-sheet-rich structures, we next incubated unstructured monomers and high molecular weight aggregates with the fluorescent dye Thioflavin T (ThT) and measured their fluorescent emission at 485 nm. The small molecule ThT changes its fluorescence spectrum upon binding to amyloidogenic β-sheet-rich fibrillar structures. However, it is important to note that ThT fluorescence gets also influenced by binding to non-amyloid structures such as DNA quadruplexes, sulfated polysaccharides, and various other polymers (Groenning, 2009). Nevertheless, it is commonly used as a reporter to monitor aggregation kinetics of Aβ42 and other amyloids (Biancalana & Koide, 2010; Naiki et al., 1989) and can be used to assess β-sheet content when analyzing synthesized peptides in vitro. We observed significant ThT binding to TAMRA Aβ42/Aβ42 co-aggregates but not monomers (Figure S2B), indicating that indeed β-sheet-rich structures are formed from the TAMRA Aβ42/Aβ42 peptide mixtures in vitro. A similar result was observed when Aβ42 aggregates formed in the absence of tracer molecules were analyzed with the assays.

TABLE 1 Statistical reports table including the degrees of freedom, F (for ANOVA) or t (for t-tests) values, and p-value of statistical tests performed.

#	Data	Figure panel	Statistical test	Degrees of freedom	F/t value	p Value
1	Aβ42-TAMRA/tubulin area localization	Figure 2b	Unpaired t-test	10	14.61	0.0000000044944092
2	Aβ42-TAMRA+cytochalasin D uptake	Figure 2d	One-way ANOVA with Dunnett's post hoc test	37	32.45	0.0000000000012285
3	Aβ42-TAMRA+EIPA uptake	Figure 2e	One-way ANOVA with Dunnett's post hoc test	9	152.8	0.000000113182086
4	Aβ42-TAMRA/LAMP2 co-localization	Figure 2f	Unpaired t-test	26	24.03	<0.000000000000000001
5	Aβ42-TAMRA/Lysotracker co-localization	Figure 2g	Unpaired t-test	12	8.640	0.000001695045907
6	Polyphenol compound screen	Figure 3b	One-way ANOVA with Dunnett's post hoc test	48	14.3	0.000000000000059
7	Aβ42-TAMRA+EGCG concentration series	Figure 3c	One-way ANOVA with Dunnett's post hoc test	16	46.56	0.000000001221386
8	Aβ42-TAMRA+EGCG validation by FRA	Figure 3e	Two-way ANOVA with Dunnett's post hoc test	27	30.69	0.0000000007556349
9	Live/dead cytotoxicity assay	Figure 3f	One-way ANOVA with Sidak's post hoc test	16	13979	<0.000000000000000001
10	MTT toxicity assay	Figure 3g	One-way ANOVA with Tukey's post hoc test	11	19.97	0.000003502193698
11	Aβ42-TAMRA+EGCG derivatives (SAR analysis)	Figure 4g	One-way ANOVA with Dunnett's post hoc test	30	13.99	0.0000000001728140
12	Aβ42-TAMRA+EGCG±bafilomycin A1	Figure 5a	Unpaired t-test	10 / 12	7.827 / 1.825	0.0000142487621 55 / 0.09
13	SH-EP cathepsin B activity±bafilomycin A1	Figure 5c	One-way ANOVA with Tukey's post hoc test	9	81.96	0.0000001674090924
14	SH-EP cathepsin B activity+10/20/30/40µM EGCG	Figure 5e	One-way ANOVA with Dunnett's post hoc test	14	82.15	0.0000000001468231
15	Aβ42-TAMRA+EGCG+1/2.5/5/10µM CA074me	Figure 5f	Two-way ANOVA with Dunnett's post hoc test	39	79.21	<0.0000000000000001
16	Aβ42-HiLyte+EGCG and Rhodamine-labeled derivative	Figure 6d,e	One-way ANOVA with Dunnett's post hoc test	26	21.81	0.0000000000147917
17	Aβ42 competitive binding (EGCG/EGC-DHB-Rhb)	Figure 6e	One-way ANOVA with Dunnett's post hoc test	18	166.9	0.00000000000000003

Next, we investigated the stability of ^{TAMRA}Aβ42/Aβ42 co-aggregates using a denaturing filter retardation assay (dFRA). With this method large SDS-stable fibrillar Aβ42 aggregates, which are retained on the surface of a cellulose acetate membrane after a filtration step, can be readily quantified using Aβ-specific antibodies (Wanker et al., 1999). We found that spontaneously formed ^{TAMRA}Aβ42/Aβ42 co-aggregates are detected by dFRAs using the monoclonal anti-Aβ antibody 6E10 (Figure S2C). A similar result was obtained when the fluorescence emission of the TAMRA dye at 579 nm after excitation at 546 nm was quantified, confirming that the tracer peptides are stably incorporated into fibrillar, β-sheet-rich ^{TAMRA}Aβ42/Aβ42 co-aggregates. A comparable result was obtained when unlabeled fibrillar Aβ42 aggregates were analyzed by dFRAs (Figure S2C). As expected, preformed unlabeled Aβ42 aggregates did not emit TAMRA-specific fluorescence at 579 nm.

Finally, we assessed whether preformed fibrillar ^{TAMRA}Aβ42/Aβ42 co-aggregates are seeding-competent structures using a FP-based aggregation assay. We have previously demonstrated that this assay is highly sensitive for the detection of template-mediated Aβ42 aggregation. Also, its performance was compared and validated against state-of-the-art ThT assays (Boeddrich et al., 2019). In this assay, FP is utilized to monitor the time-dependent co-aggregation of Aβ42 monomers (10 μM) in the presence of ^{FAM}Aβ42 (0.05 μM) tracer molecules in 384-well plates. We added 80 nM (monomer equivalent) of preformed fibrillar ^{TAMRA}Aβ42/Aβ42 co-aggregates as well as unlabeled Aβ42 fibrils as sonicated seeds to aggregation reactions and monitored their impact on ^{FAM}Aβ42/Aβ42 co-polymerization. We found that through the addition of both types of fibrillar Aβ42 aggregates (TAMRA-labeled and unlabeled), the lag phase was significantly shortened (Figure S2D), indicating that the incorporation of trace amounts of TAMRA-labeled Aβ42 peptides into Aβ42 fibrils does not prevent their seeding activity. Importantly, the shortening of the lag phase observed for 80 nM of sonicated seeds was similar to the reported results, confirming our previous studies (Boeddrich et al., 2019). Together these investigations indicate that preformed fibrillar ^{TAMRA}Aβ42/Aβ42 co-aggregates have similar biochemical properties than homogenous, fibrillar Aβ42 aggregates, which are formed in the absence of tracer peptides.

3.2 | Fibrillar ^{TAMRA}Aβ42/Aβ42 co-aggregates are efficiently taken up into neuroblastoma cells

We next investigated whether preformed fibrillar ^{TAMRA}Aβ42/Aβ42 co-aggregates are taken up into neuroblastoma cells when they are added to the culture medium. We incubated SH-EP cells for 2, 4, 6, and 8 h with ^{TAMRA}Aβ42/Aβ42 co-aggregates (600 nM). After washing and trypsinization to remove extracellular membrane-bound co-aggregates, cells were analyzed by fluorescence microscopy (FM). We observed a time-dependent increase of TAMRA-positive foci, when SH-EP cells were treated with ^{TAMRA}Aβ42/Aβ42 co-aggregates

(magenta spots, Figure 1a), indicating that fluorescently labeled fibrillar Aβ42 structures are readily taken up into mammalian cells. Very similar results were obtained when cells were stained with the anti-Aβ antibody 6E10 (green spots, Figure 1a), confirming the results by immunocytochemistry. We detected smaller as well as larger TAMRA-positive and antibody signals in cells, suggesting that aggregates with different sizes are incorporated into SH-EP cells and are detected by both readouts (Figure 1b). When TAMRA- and 6E10-positive signals were compared, we found that both signals correlate well and increase over time in SH-EP cells (Figure 1c).

Next, SH-EP cells harboring ^{TAMRA}Aβ42/Aβ42 co-aggregates were stained with the fluorescent dye ThS, which similar to ThT binds to β-sheet-rich amyloid fibrils and other polymers, but not to Aβ monomers (Kelényi, 1967). We observed significant co-localization of ThS and TAMRA fluorescence in cytoplasmic inclusion bodies in SH-EP cells (Figure 1d), indicating that the intracellular TAMRA-labeled Aβ42 aggregates are ThS-positive, similar to previously reported in vivo Aβ aggregates (Kelényi, 1967).

To biochemically confirm the presence of cellular Aβ42 aggregates, SH-EP cells were lysed after 2, 4, 6, and 8 h of treatment with ^{TAMRA}Aβ42/Aβ42 co-aggregates and protein extracts were analyzed using a native (nFRA, 0.1% NP40) and a denaturing filter assay (dFRA, 2% SDS), which exclusively detects large SDS- and heat-stable amyloid aggregates retained on filter membranes (Wanker et al., 1999). Quantified from the TAMRA fluorescence intensities of retained aggregates on filter membranes, we measured a time-dependent increase of Aβ42 aggregates with nFRAs (NP40, Figure 1e) and dFRAs (SDS, Figure 1e), confirming our hypothesis that highly stable, β-sheet-rich amyloid aggregates are taken up and accumulate in SH-EP cells. The accumulation of high-molecular-weight SDS-stable structures upon treatment of cells with preformed fibrillar Aβ42 aggregates was also confirmed by SDS-PAGE and immunoblotting. In Aβ42 aggregate-treated cells both high molecular weight aggregates (migrating in the stacking gel) and monomers (migrating at ~4 kDa) were detectable (+Aβ42 aggregates, Figure 1f), indicating that at least a fraction of the incorporated, intracellular Aβ42 aggregates are sensitive to SDS and heat and can be dissociated into monomers. In contrast, such structures were non-detectable in SH-EP cells that were treated with soluble Aβ42 peptides, suggesting that unstructured Aβ42 monomers (Baumketner et al., 2006) in contrast to preformed β-sheet-rich aggregates are either efficiently degraded or not internalized by SH-EP cells (+Aβ42 monomer, Figure 1f).

3.3 | Fibrillar ^{TAMRA}Aβ42/Aβ42 co-aggregates are internalized by macropinocytosis and accumulate in lysosomes in SH-EP cells

To distinguish a potential intracellular from an extracellular accumulation of ^{TAMRA}Aβ42/Aβ42 co-aggregates, we first co-stained TAMRA signals with a tubulin marker protein, which stains a complex network of microtubules in the cytoplasm of SH-EP cells (Figure 2a).
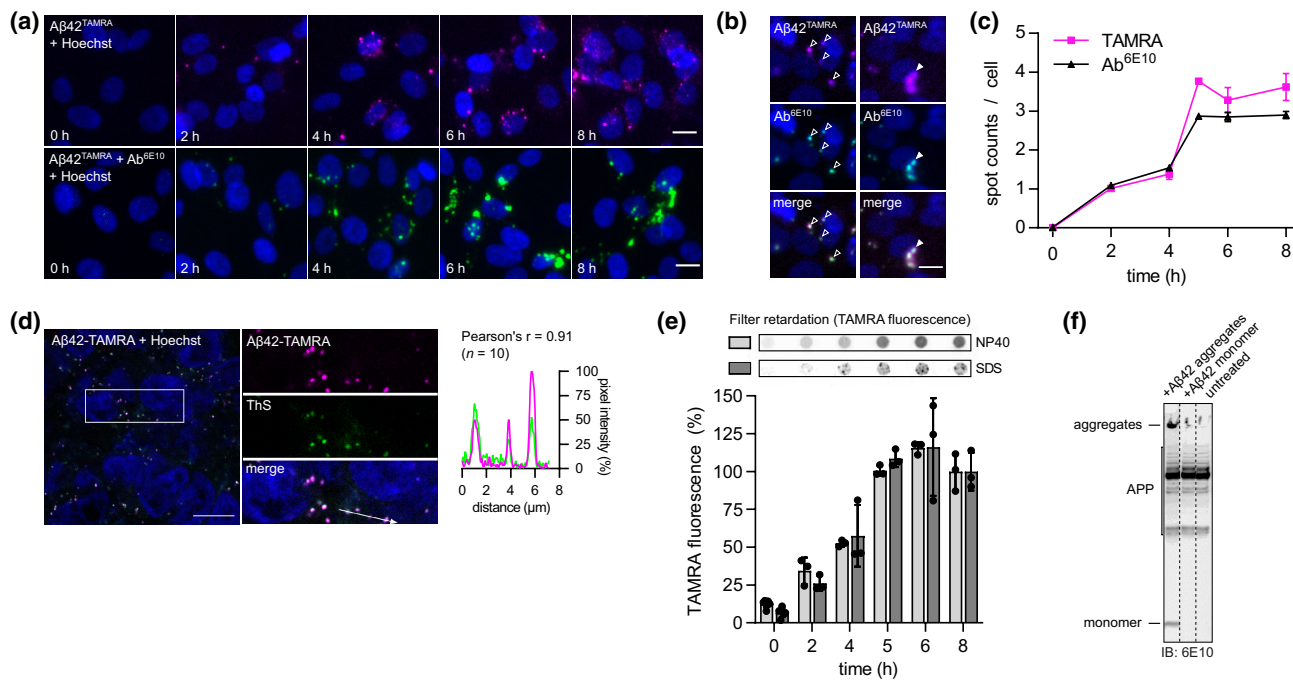
FIGURE 1 ^{TAMRA}Aβ42/Aβ42 co-aggregates are internalized by SH-EP cells. (a) Images from automated microscopy of SH-EP cells treated with 600 nM ^{TAMRA}Aβ42/Aβ42 co-aggregates for indicated times. Cells were fixed and nuclei stained with Hoechst 33342 (*blue*); ^{TAMRA}Aβ42/Aβ42 co-aggregates are indicated by magenta-colored spots (upper panel). Cells with ^{TAMRA}Aβ42/Aβ42 co-aggregates were additionally immunostained with the Aβ-specific antibody 6E10 and a fluorescently labeled secondary antibody. Antibody-detected ^{TAMRA}Aβ42/Aβ42 co-aggregates are indicated by green-colored fluorescent spots (lower panel). Scale bars: 15 µm. (b) Direct comparison of TAMRA signals of intracellular ^{TAMRA}Aβ42/Aβ42 co-aggregates and immunostainings of SH-EP cells with the 6E10 antibody (Ab^{6E10}). Aggregates identified by TAMRA signals are also detected with 6E10 immunostainings. Both small (left images) and large TAMRA-positive ^{TAMRA}Aβ42/Aβ42 co-aggregates (right images) are detectable. (c) Quantification of TAMRA (magenta rectangles) and 6E10-positive spots per cell (black triangles) at indicated time points using automated microscopy and spot detection. Data points represent mean values ± SD from three independent cell culture preparations (n = 3) analyzed in technical triplicates. (d) Confocal microscopy of cellular ^{TAMRA}Aβ42/Aβ42 co-aggregates stained with thioflavin S (ThS, *green*). Cell nuclei are stained with Hoechst33342 (*blue*). Line plot profile displays the fluorescence intensity of ThS (*green*) and TAMRA (*magenta*) along the white arrow. Pearson's correlation coefficient (*r*) is used to determine co-localization of TAMRA and ThS fluorescence intensity. Scale bar: 10 µm. Representative region of interest (ROI) and co-localization analysis are shown. In total, 10 ROIs (n = 10) from 10 individual cells were analyzed resulting in mean Pearson's *r* of 0.91. (e) Denaturing (SDS) and non-denaturing (NP40) filter retardation assays (dFRA, nFRA) of SH-EP cell lysates determining aggregate content after incubation with ^{TAMRA}Aβ42/Aβ42 co-aggregates for indicated times. Retained aggregates were quantified from TAMRA fluorescence intensities normalized to content maximum after 6 h. Data points represent mean values ± SD from three independent filter assays (n = 3). (f) Western blot of SH-EP cell lysates after incubation with ^{TAMRA}Aβ42/Aβ42 co-aggregates for 6 h. Aggregate-treated cells show SDS-stable 6E10-positive aggregates in gel pockets and a monomeric Aβ peptide band. Monomer-treated cell lysate or untreated cell lysate do not show aggregates in gel pockets or a monomeric Aβ peptide band. 6E10 antibody also detects endogenous APP in SH-EP cells.

By performing a segmentation analysis to determine the amount of ^{TAMRA}Aβ42/Aβ42 co-aggregates co-localizing with the cell body defined by tubulin staining, we found that >80% of the Aβ42-TAMRA signal is within the tubulin-positive area (Figure 2b), supporting our hypothesis that ^{TAMRA}Aβ42/Aβ42 co-aggregates accumulate intracellularly in SH-EP cells. To further validate that ^{TAMRA}Aβ42/Aβ42 co-aggregates are internalized and do not primarily stick to the outer membrane, we also performed z-stack analyses. A representative z-stack image of 0.9 µm through the cell body is shown in Figure 2c. We found that the vast majority of detected ^{TAMRA}Aβ42/Aβ42 co-aggregates are indeed adjacent to the microtubule network, indicating their intracellular localization at cytoplasmic cytoskeletal structures.

Previous investigations have shown that aggregation-prone Aβ peptides are internalized by actin-dependent endocytotic processes (Lai & McLaurin, 2010). We, therefore, investigated whether the uptake of ^{TAMRA}Aβ42/Aβ42 co-aggregates into SH-EP cells is dependent on actin polymerization. We treated SH-EP cells with the actin polymerization inhibitor cytochalasin D (May et al., 1998) and analyzed cellular lysates after 6 h of treatment with ^{TAMRA}Aβ42/Aβ42 co-aggregates using a dFRA. We found that cytochalasin D treatment leads to a concentration-dependent reduction of the cellular Aβ42 aggregate content, indicating that the uptake process in SH-EP cells is dependent on actin polymerization (Figure 2d). An actin-dependent, fluid-phase uptake process termed macropinocytosis was previously described to mediate Aβ42 internalization. Also, this process was implicated in the propagation of protein aggregates (Zeineddine & Yerbury, 2015). To investigate whether SH-EP cells internalize ^{TAMRA}Aβ42/Aβ42 co-aggregates via this pathway, we next
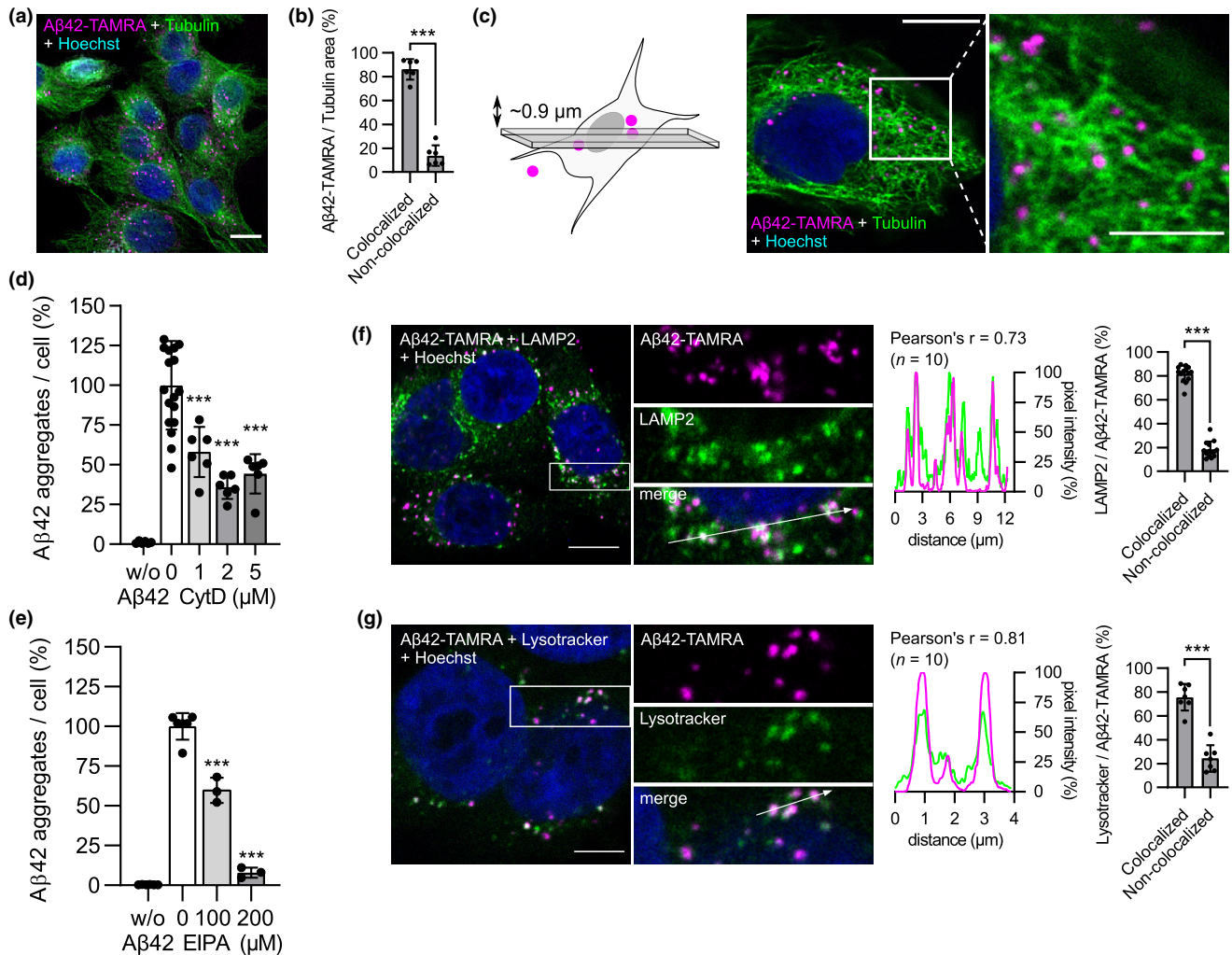
FIGURE 2 TAMRAAβ42/Aβ42 co-aggregates are internalized by actin-dependent macropinocytosis and accumulate in lysosomes. (a) SH-EP cells were treated with TAMRAAβ42/Aβ42 co-aggregates for 6 h, washed, trypsinized, re-plated, and stained with Hoechst and an anti-tubulin antibody. Scale bar: 10 μm. (b) SH-EP cell bodies were segmented from tubulin signals to discriminate between extracellular (non-colocalized) and intracellular aggregates (colocalized). Bar plot shows co-localization analysis of multiple image sections ($n = 6$). Co-localization was quantified according to Costes et al. (2004) in % TAMRA intensity co-localized with tubulin segmented area. Unpaired t-test, ***$p < 0.001$. (c) Scheme and representative image of z-stack analysis performed to validate intracellular localization of TAMRAAβ42/Aβ42 co-aggregates. Optical section thickness was ~0.9 μm. Scale bars: 10 μm. (d) SH-EP cells were treated with TAMRAAβ42/Aβ42 co-aggregates for 6 h and increasing concentrations of actin polymerization inhibitor cytochalasin D (CytD). Cell lysates were analyzed by dFRAs and aggregate content was quantified from TAMRA fluorescence intensities. Bars represent mean values ± SD from two cell culture preparations ($n = 2$). One-way ANOVA with Dunnett's post hoc test, ***$p < 0.001$. (e) Intracellular TAMRAAβ42/Aβ42 co-aggregates after pretreatment of SH-EP cells with macropinocytosis inhibitor ethyl-isopropyl amiloride (EIPA). Internalized Aβ42 aggregate load was quantified from total TAMRA spot area per cell. Bars represent mean values ± SD from three independent cell culture preparations ($n = 3$). One-way ANOVA with Dunnett's post hoc test, ***$p < 0.001$. (f) Confocal microscopy of SH-EP cells with TAMRAAβ42/Aβ42 co-aggregates co-localizing with lysosomal-associated membrane protein 2 (LAMP2). Line plot profile displays the fluorescence intensity of LAMP2 antibody signals (*green*) and TAMRA (*magenta*) along white arrow. Pearson's correlation coefficient (r) is used to determine co-localization of TAMRA and LAMP2 signal intensities. Cell nuclei are stained with Hoechst 33342 (*blue*). Scale bar: 10 μm. Representative ROI and co-localization analysis are shown. In total, 10 ROIs ($n = 10$) from 4 individual cells were analyzed resulting in mean Pearson's r of 0.73. Bar plot shows co-localization analysis of multiple image sections ($n = 14$). Co-localization was quantified according to Costes et al. (2004) in % TAMRA intensity co-localized with LAMP2 signal intensity. Bars represent mean values ± SD, unpaired t-test, ***$p < 0.001$. (g) Confocal microscopy of cellular TAMRAAβ42/Aβ42 co-aggregates with Lysotracker staining. Cell nuclei are stained with Hoechst 33342 (*blue*). Line plot profile displays the fluorescence intensity of Lysotracker (*green*) and TAMRA (*magenta*) along white arrow. Pearson's correlation coefficient (r) is used to determine co-localization of TAMRA and Lysotracker fluorescence intensity. Scale bar: 5 μm. Representative region of interest (ROI) and co-localization analysis are shown. In total, 10 ROIs ($n = 10$) from 5 individual cells were analyzed resulting in mean Pearson's r of 0.81. Bar plot shows co-localization analysis of multiple image sections ($n = 7$). Co-localization was quantified according to Costes et al. (2004) in % TAMRA intensity co-localized with Lysotracker signal intensity.
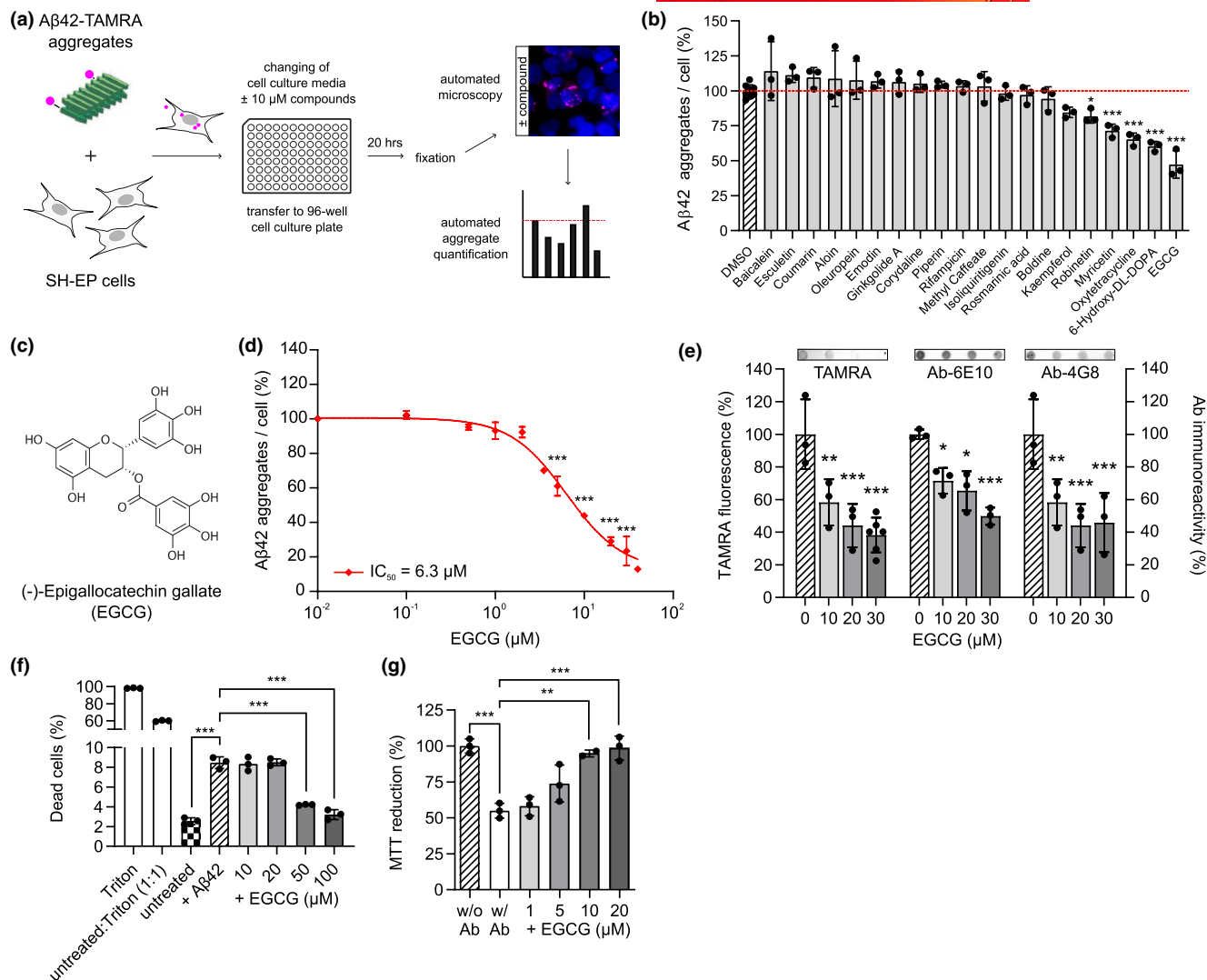
FIGURE 3 The polyphenolic compound EGCG reduces the abundance of preformed ^{TAMRA}Aβ42/Aβ42 co-aggregates and decreases toxicity in SH-EP cells. (a) Scheme of cell-based screening assay. SH-EP cells are treated with preformed ^{TAMRA}Aβ42/Aβ42 co-aggregates, extracellular aggregates are removed by extensive washing and trypsinization, and cells are seeded onto 96-wells with polyphenolic compounds (10 μM) in technical triplicates. After 20 h, cells are fixed, Hoechst 33342 stained, and automated microscopy and aggregate quantification is performed. (b) SH-EP cells with ^{TAMRA}Aβ42/Aβ42 co-aggregates were treated with 10 μM polyphenolic compounds. Aggregates were quantified after 20 h of incubation from total TAMRA spot counts per cell and normalized to solvent (DMSO) control. Bars represent mean values ± SD compared to DMSO control from three individual cell culture preparations ($n = 3$) analyzed in technical triplicates. One-way ANOVA with Dunnett's post hoc test, $*p < 0.05$, $***p < 0.001$. (c) Chemical structure of most potent ^{TAMRA}Aβ42/Aβ42 co-aggregates reducing compound (EGCG). (d) Concentration-dependent reduction of intracellular Aβ42 aggregates after 20 h of EGCG treatment. EGCG reduced cellular Aβ42 aggregate load per cell with an IC$_{50}$ of 6.3 μM. Data points represent mean values ± SD compared to DMSO control from independent cell culture preparations ($n = 3$) analyzed in technical triplicates. One-way ANOVA with Dunnett's post hoc test, $***p < 0.001$. (e) Validation of EGCG-mediated intracellular aggregate reduction with native filter retardation assays. SH-EP cells with ^{TAMRA}Aβ42/Aβ42 co-aggregates were lysed and analyzed 20 h after incubation with EGCG or solvent control. Aggregate load of cell lysates was quantified from TAMRA signals or by immunostaining using two Aβ-specific antibodies (Ab-6E10, Ab-4G8). Bars represent mean values ± SD compared to DMSO control from three filter assays ($n = 3$). One-way ANOVA with Dunnett's post hoc test, $*p < 0.05$, $**p < 0.01$, $***p < 0.001$. (f) Treatment of SH-EP cells with 1 μM preformed Aβ42 aggregates increases the relative proportion of dead cells (Live/Dead toxicity) indicating Aβ-induced toxicity (untreated vs. +Aβ42). The addition of increasing concentrations of EGCG reduces the proportion of dead cells (+Aβ42 + 50 or 100 μM EGCG). Bars represent mean values ± SD from one representative experiment performed in triplicate. One-way ANOVA with Sidak's post hoc test, $***p < 0.001$. (g) SH-EP cells treated with 1 μM Aβ42 aggregates show increased toxicity as measured by reduced MTT reduction (untreated vs. +Aβ42). EGCG treatment rescues Aβ42 aggregate-induced toxicity. Bars represent mean values ± SD from three independent cell culture preparations ($n = 3$). One-way ANOVA with Tukey's post hoc test, $*p < 0.05$, $**p < 0.01$, $***p < 0.001$.

applied the macropinocytosis inhibitor ethyl-isopropyl amiloride (EIPA) and monitored Aβ42 aggregate uptake by determining the Aβ42-TAMRA spot area per cell. With 100 μM EIPA, the regions of TAMRA-positive spots per cell were reduced to ~50%, while treatment with 200 μM EIPA almost completely abolished the detection of TAMRA Aβ42/Aβ42 co-aggregates in SH-EP cells (Figure 2e).

After uptake, Aβ42 aggregates were previously reported to accumulate in acidic vesicles such as late endosomes or lysosomes (Knauer et al., 1992; Marshall et al., 2020). Therefore, we next wanted to assess, whether TAMRA-labeled Aβ42 aggregates may also be concentrated in such intracellular compartments in SH-EP cells. To address this, we incubated SH-EP cells for 6 h with preformed TAMRA Aβ42/Aβ42 co-aggregates and after washing, trypsinization, and re-plating, we co-stained the cells with an antibody against the lysosome-associated membrane protein 2 (LAMP2), a protein previously used as a marker for lysosomes in mammalian cells (Chen et al., 1985; Eskelinen et al., 2002). We observed significant co-localization between TAMRA Aβ42/Aβ42 co-aggregates and LAMP2-positive membrane vesicles and found that ~80% of the TAMRA Aβ42/Aβ42 co-aggregates co-localize with LAMP2-positive subcellular compartments (Figure 2f), suggesting that they accumulate in lysosomes and/or late endosomes in SH-EP cells. Similar results were obtained when cells with TAMRA Aβ42/Aβ42 co-aggregates were co-stained with Lysotracker probes, which consist of a fluorophore linked to a weak base that is protonated and retained in the lumina of acidic vesicles (Wood, 1994). Here, we found that >75% of the detected TAMRA Aβ42/Aβ42 co-aggregates co-localize with Lysotracker spots, suggesting that the internalized Aβ42 aggregates are present in lysosomes (Figure 2g). To investigate whether the TAMRA Aβ42/Aβ42 co-aggregates are also detectable in lysosomes biochemically, we additionally enriched lysosomes from crude protein extracts of SH-EP cells. Successful enrichment of lysosomes was confirmed by an increase of the lysosome-associated membrane protein 1 (LAMP1) in the lysosomal fraction compared to total protein content (Figure S3A). In contrast, flotilin-1, a membrane protein not specifically enriched in lysosomes (Bickel et al., 1997), showed reduced levels in the prepared lysosomal fraction (Figure S3B). Using the 6E10 antibody, we could detect SDS-stable Aβ42 co-aggregates (in the stacking gel) as well as monomeric Aβ42, likely released from non-SDS-stable aggregates, in the lysosomal fraction of TAMRA Aβ42/Aβ42 co-aggregate-treated samples, while no such signals were observed in untreated cells (Figure S3C). Additionally, we found Aβ42 aggregates to sporadically localize to the nucleus (Figure 2f,g), which is in agreement with previously reported studies where Aβ42 peptides were expressed in the endoplasmic reticulum (Bückig et al., 2002).

3.4 | The polyphenolic compound EGCG reduces the abundance of preformed TAMRA Aβ42/Aβ42 co-aggregates and ameliorates their toxicity in SH-EP cells

To identify small molecules that target amyloid aggregates and promote their degradation in cells, we next established a compound screening assay in 96-well microtiter plates (Figure 3a) and systematically tested 20 polyphenolic compounds for their effects on preformed TAMRA Aβ42/Aβ42 co-aggregates in SH-EP cells. We focused our efforts on polyphenolic compounds because previous in vitro studies have demonstrated that such structures directly associate with amyloidogenic peptides and are able to modulate their biochemical properties (Ehrnhoefer et al., 2006; Gazova et al., 2013; Matos et al., 2017; Ono et al., 2003). Furthermore, effects of polyhydroxyphenoles on protein degradation pathways have been described (Liberal et al., 2014; Modernelli et al., 2015; Regitz et al., 2014), suggesting that they might stimulate the clearance of amyloid aggregates in cells via protein degradation pathways. We found that of 20 tested chemical compounds 5 (robinetin, myricetin, oxytetracycline, 6-hydroxy-DL-DOPA, and EGCG) significantly decreased the abundance of TAMRA Aβ42/Aβ42 co-aggregates in SH-EP cells. Strikingly, the strongest effect was observed with EGCG ((−)-epigallocatechin gallate; Figure 3b,c), which at a concentration of 10 μM caused a reduction of intracellular Aβ42 aggregate load by >50%. This effect was also confirmed when the compound was assessed in cell-based assays in a concentration-dependent manner. As shown in Figure 3d, EGCG treatment decreased the abundance of TAMRA Aβ42/Aβ42 co-aggregates with an IC_{50} of ~6 μM. Importantly, none of the identified hit compounds showed an effect on the fluorescence intensity of the TAMRA fluorophore alone (Figure S4A).

Next, we validated the EGCG-mediated reduction of amyloidogenic Aβ42 aggregates in SH-EP cells using filter retardation assays. We incubated cells for 6 h with preformed TAMRA Aβ42/Aβ42 co-aggregates (1 μM monomer equivalent) to promote aggregate uptake. Subsequently, cells were trypsinized, replated, and incubated with 10, 20, and 30 μM EGCG for 20 h to stimulate aggregate degradation. Finally, cells were lysed and protein extracts were analyzed by filter retardation assays. Compared to untreated controls, we observed a concentration-dependent decrease of TAMRA fluorescent protein aggregates in EGCG-treated samples (Figure 3e), indicating that compound treatment reduces intracellular Aβ42 aggregate load. A similar result was obtained when the cellular aggregates were immunodetected using the monoclonal anti-Aβ antibodies 6E10, which binds to Aβ's N-terminus (Sloane et al., 1997), and 4G8, which specifically recognizes amino acids 17–22 in the Aβ peptide (Hatami et al., 2014) and has an amyloid-specific epitope (Hatami et al., 2016). Together, these studies indicate that EGCG potently decreases the abundance of intracellular SDS-stable, β-sheet-rich Aβ42 aggregates in neuroblastoma cells.

We additionally investigated whether EGCG treatment can reduce Aβ42 aggregate-induced toxicity in cells. Therefore, we first performed a Live/Dead cytotoxicity assay, which was previously used to investigate Aβ-induced toxicity (Konar et al., 2022; Vadukul et al., 2020). It detects dead cells by quantifying the hydrolysis of calcein-AM to calcein and through quantification of cell permeability by propidium iodide staining. SH-EP cells were treated with 1 μM preformed Aβ42 aggregates for 6 h and subsequently with increasing concentrations of EGCG for 20 h. As a control, we also treated SH-EP cells without Aβ with increasing concentrations of

EGCG or with 0.05% Triton-X100. A 1:1 mixture of untreated and Triton-X100-treated cells was used to determine the gate for quantifying the proportion of dead cells (Figure S4B). We found that the addition of preformed Aβ42 aggregates to SH-EP cells increases the proportion of dead SH-EP cells, while the co-treatment with 50 or 100μM EGCG significantly reduces this Aβ-induced toxicity (Figure 3f). As an additional toxicity assay, we used a standardized colorimetric 3-(4,5-dimethylthiazol-2-yl)-2,5-diphenyltetrazolium bromide (MTT) reduction assay to examine whether EGCG treatment influences the mitochondria-associated toxicity of preformed Aβ42 aggregates in SH-EP cells. We incubated cells in 96-well plates with 1μM preformed fibrillar β-sheet-rich Aβ42 aggregates for 6h in order to facilitate efficient aggregate uptake. Subsequently, cells were incubated for 20h with EGCG to stimulate aggregate degradation. Finally, MTT reduction was quantified to monitor mitochondrial toxicity. We found that β-sheet-rich fibrillar Aβ42 aggregates (+Aβ42) cause a pronounced and significant inhibition of MTT reduction (~50%, Figure 3g), while this mitochondrial dysfunction was diminished in a concentration-dependent manner when cells were treated with increasing concentrations of EGCG. Thus, our toxicity data indicate that EGCG reduces the Aβ42-induced mitochondrial dysfunction as well as impairment of cell integrity, which is detected with the Live/Dead toxicity assay. In summary, this indicates that an EGCG-stimulated reduction of β-sheet-rich fibrillar Aβ42 aggregates in mammalian cells is associated with reduced cellular toxicity.

3.5 | Effects of EGCG derivatives on the abundance of preformed Aβ42 aggregates
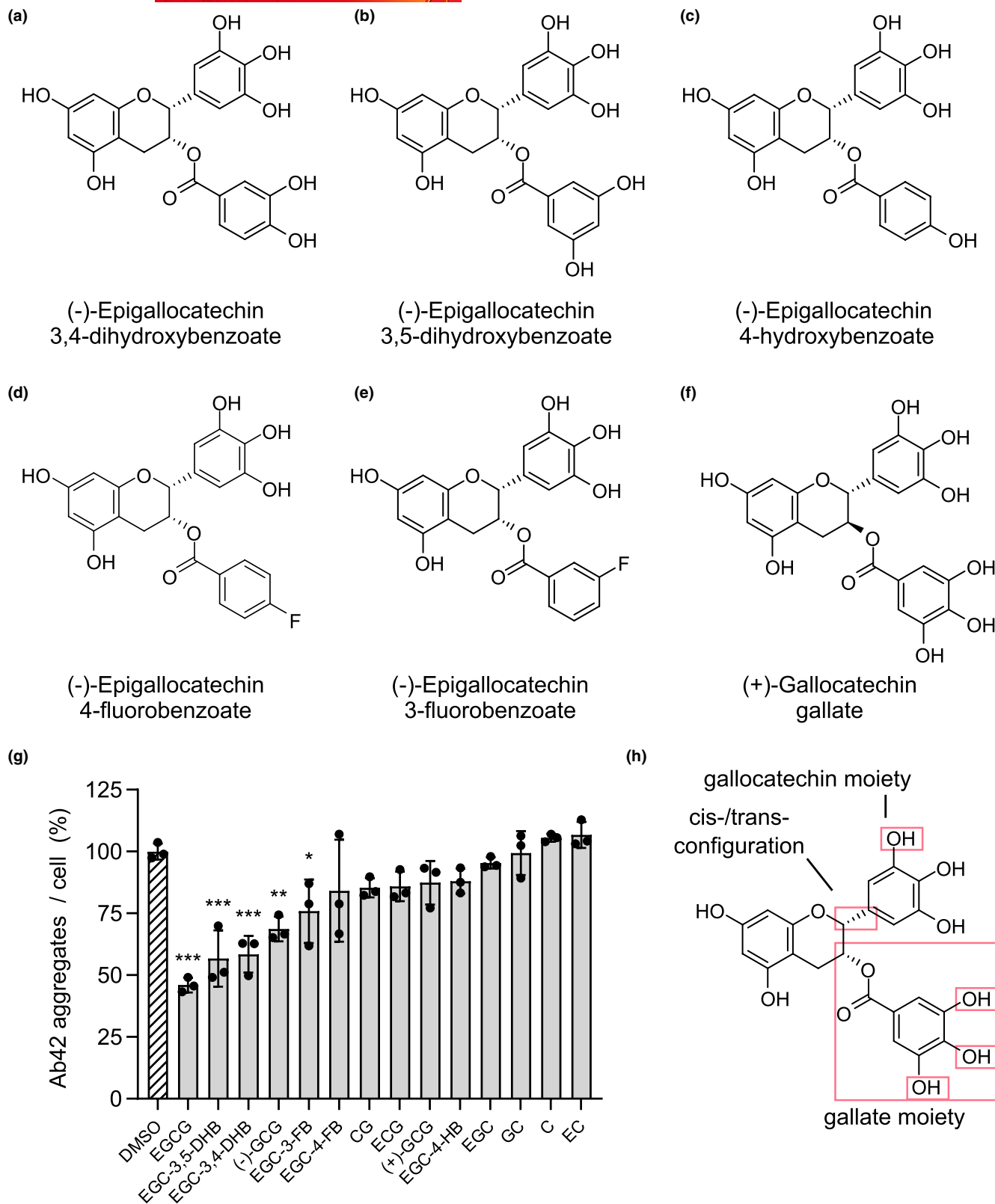
EGCG is the ester of epigallocatechin and gallic acid (Kada et al., 1985), which has three hydroxy groups that might be required for the interaction with preformed Aβ42 aggregates in cells. We synthesized 5 EGCG-related small molecules with reduced numbers of hydroxy groups (EGC-3,4-DHB, EGC-3,5-DHB, EGC-3-HB, EGC-3-FB, and EGC-4-FB, Figure 4a–e) and a trans-configured epimer of EGCG ((+)-GCG, Figure 4f) and subsequently assessed their impact on preformed TAMRAAβ42/Aβ42 co-aggregates in SH-EP cells. In addition, the impact of the previously described green tea compounds (−)-epigallocatechin (EGC), (−)-gallocatechin (GC), epicatechin (EC), and (−)-catechin (C), which lack the gallate group; epicatechin gallate (ECG) and its epimer catechin gallate (CG), which lack the C5 hydroxy group in the chroman moiety; and the epimer of EGCG, (−)-GCG, were investigated (Table S1). While the compounds EGC-3,5-DHB and EGC-3,4-DHB with a dihydroxybenzoate group still showed a strong Aβ42 aggregate-clearing effect, it was diminished with the compound EGC-4-HB, which contains only a single hydroxy group on the benzoate moiety. A reduced Aβ42 aggregate-clearing potency was also observed for the compounds EGC-3-FB and EGC-4-FB, which both contain a single fluorobenzoate moiety, as well as with the compounds EGC, GC, and C, which completely lack the gallate moiety (Figure 4g). Thus, our data suggest that the number of free hydroxy groups in the gallate moiety is critical for the effect of EGCG

on TAMRAAβ42/Aβ42 co-aggregates in cells. Additionally, we found that the hydroxy group on C5 in the chroman moiety is important for intracellular Aβ42 aggregate reduction (Figure 4g; EGCG, ECG) and that the trans-configured epimers in comparison to EGCG show a reduced activity (Figure 4g; EGCG, (−)-GCG, (+)-GCG). Taken together, our structure–activity relationship (SAR) analysis indicates that the free hydroxy groups in the gallate and chroman moieties, and the cis/trans configuration influence EGCG's Aβ42 aggregate-reducing activity in SH-EP cells. An overview of the substructures that influence EGCG activity in cell-based assays is given in Figure 4h.

Since it was previously described that EGCG might be hydrolytically and oxidatively instable at neutral pH wherefore degradation products could be the actual effective substances (Palhano et al., 2013; Sternke-Hoffmann et al., 2020), we analyzed whether EGCG is stable during the time course of the assay. The stability of catechins, including EGCG, in acidic solutions, has been investigated earlier (Chen et al., 1998; Proniuk et al., 2002; Zhu et al., 1997). These studies revealed that catechins generally show a good stability at or below pH5.5. Therefore, it seems feasible to speculate that EGCG in lysosomes should be rather stable. However, in the cytoplasm or in the culture medium where the pH is neutral, it might undergo hydrolysis or oxidation. In order to evaluate the stability of EGCG and CG at pH6.0 and pH7.4 measurements were performed with NMR and ultraviolet–visible (UV–Vis) spectroscopy over a period of 24h at 37 °C (see stability studies of gallocatechin and catechin derivatives, Supporting Information). We found that hydrolysis of the gallate moiety in both EGCG and CG under these conditions was not detectable. In the NMR spectrum of EGCG new signals appeared after 24h which were mostly attributed to the epimer GCG (Hayashi & Ujihara, 2017; Ishizu et al., 2009), but the amount was below 1%. The NMR spectrum of CG showed no formation of degradation products. Additionally, the exposure to air and concomitant irradiation with blue light allowed us to check for photochemically-induced oxidation of the electron-rich aromatic moiety. Prolonged irradiation of an air-saturated solution of EGCG by blue LED light of high intensity (for 19h in a photoreactor) led to a light peach coloration of the solution and slightly increased absorption in the UV–Vis spectra (UV–Vis-Studies, Supporting Information). However, also in this case the corresponding NMR spectra showed no substantial change by formation of degradation products for both catechins (NMR-Studies, Supporting Information). These analyses indicate that the investigated catechin derivatives are stable for the duration of the assay studies and that the results are representative of the compounds indicated.

3.6 | EGCG treatment increases the maturation and the enzymatic activity of cathepsin B in SH-EP cells

Our study indicates that preformed fibrillar Aβ42 aggregates accumulate in lysosomes (Figure 2f,g), suggesting that lysosome function might be critical for EGCG-mediated aggregate degradation in cells.

(a) (-)-Epigallocatechin 3,4-dihydroxybenzoate

(b) (-)-Epigallocatechin 3,5-dihydroxybenzoate

(c) (-)-Epigallocatechin 4-hydroxybenzoate

(d) (-)-Epigallocatechin 4-fluorobenzoate

(e) (-)-Epigallocatechin 3-fluorobenzoate

(f) (+)-Gallocatechin gallate

(g)

(h)

gallocatechin moiety

cis-/trans-configuration

gallate moiety

Lysosomes have a specific composition, of both their membrane and luminal proteins, and it was shown that a luminal pH of ~5 is optimal for enzymes involved in protein hydrolysis. Evidence was presented that the activity of the vacuolar-type H+ ATPase (V-ATPase) is critical for lysosome function and its acidification (Mindell, 2012), suggesting that its inhibition through the compound bafilomycin A1

(Mauvezin & Neufeld, 2015) may influence EGCG-mediated degradation of Aβ42 aggregates in cells. To address this question, we incubated SH-EP cells, which contain preformed fibrillar ^{TAMRA}Aβ42/Aβ42 co-aggregates, with EGCG and 10 nM bafilomycin A1 for 20 h and subsequently measured the aggregate load by quantifying TAMRA fluorescence using automated fluorescence microscopy.
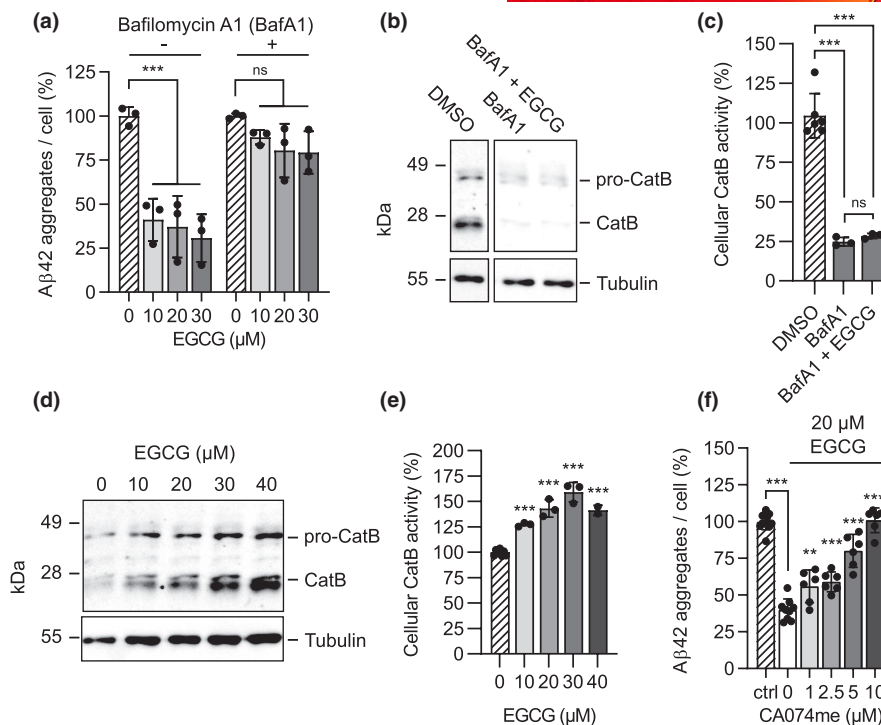
FIGURE 5 EGCG increases cathepsin B maturation and enzymatic activity in SH-EP cells. (a) SH-EP cells with intracellular Aβ42 aggregates treated with 10, 20, and 30 μM EGCG in presence (+) and absence (−) of 10 nM bafilomycin A1. Aggregates were quantified from total TAMRA spot counts per cell. Bars represent mean values ± SD compared to DMSO (0) control from three independent cell culture preparations (n = 3) analyzed in technical triplicates. Two-way ANOVA with Bonferroni's post-test, ***$p < 0.001$, ns, not significant. (b) Western blot of cellular extracts of SH-EP cells treated with 10 nM bafilomycin A1 only and 10 nM bafilomycin A1 + 20 μM EGCG. Cathepsin B pro-enzyme (pro-CatB) and its maturated form (CatB) are detected. Tubulin was used as a loading control. Bafilomycin-treated SH-EP cells show no substantial cathepsin B maturation. EGCG does not rescue CatB maturation. Note: The contrast of the images was adjusted and an average background value was subtracted. All image areas were processed similarly. (c) Cathepsin B activity in SH-EP cell extracts after treatment with bafilomycin A1 (10 nM) or DMSO as control. CatB activity was measured in SH-EP cell lysate after the addition of fluorescence quenching CatB substrate Z-Arg-Arg 7-amido-4-methylcoumarin (Z-R-R-AMC). Bars represent mean values from three independent lysate preparations (n = 3). One-way ANOVA with Dunnett's post hoc test, ***$p < 0.001$. (d) Western blot of cellular extracts of SH-EP cells treated with increasing concentrations of EGCG. Cathepsin B pro-enzyme (pro-CatB) and its maturated form (CatB) are detected. Tubulin was used as a loading control. Note: The contrast of the images was adjusted and an average background value was subtracted. All image areas were processed similarly. (e) CatB activity in SH-EP cell lysates after treatment with EGCG for 20 h. CatB activity was quantified using a fluorescence-quenched substrate (Z-R-R-AMC) assay. Bars represent means from three independent cell lysate preparations (n = 3). One-way ANOVA with Dunnett's post hoc test, ***$p < 0.001$. (f) Treatment of cells with cathepsin B inhibitor CA074me counteracts cellular degradation of TAMRAAβ42/Aβ42. SH-EP cells with intracellular Aβ42 aggregates treated with EGCG (20 μM) and increasing concentrations of CA074me. After 20 h aggregates were quantified from total TAMRA spot counts per cell. Bars represent means ± SD from three independent cell culture preparations (n = 3) analyzed in technical triplicates. Two-way ANOVA with Dunnett's post-test, *$p < 0.05$, **$p < 0.01$, ***$p < 0.001$. CA04me treated samples were compared to untreated control (0 μM).

As observed previously, we found that EGCG treatment in the absence of bafilomycin A1 significantly decreased the abundance of TAMRAAβ42/Aβ42 co-aggregates (− bafilomycin A1, Figure 5a). In strong contrast, in the presence of the V-ATPase inhibitor, the effect of EGCG on TAMRAAβ42/Aβ42 co-aggregates was dramatically diminished (+ bafilomycin A1, Figure 5a). This indicates that lysosomal

FIGURE 4 Structures of newly synthesized EGCG derivatives and structure–activity relationship (SAR) analysis. (a) Structure of (−)-epigallocatechin 3,4-dihydroxybenzoate, an EGCG derivative lacking the C5 hydroxy group of the gallate moiety. (b) Structure of (−)-epigallocatechin 3,5-dihydroxybenzoate, an EGCG derivative lacking the C4 hydroxy group of the gallate moiety. (c) Structure of (−)-epigallocatechin 4-hydroxybenzoate, an EGCG derivative lacking the C3 and C5 hydroxy groups of the gallate moiety. (d) Structure of (−)-epigallocatechin 4-fluorobenzoate, an EGCG derivative lacking the C3 and C5 hydroxy groups, with substitution of the C4 hydroxy group by fluorine on the gallate moiety. (e) Structure of (−)-epigallocatechin 3-fluorobenzoate, an EGCG derivative lacking the C4 and C5 hydroxy groups with substitution of the C3 by fluorine on the gallate moiety. (f) Structure of (+)-gallocatechin gallate, a trans-configured epimer of EGCG. (g) SAR using newly synthesized and previously published EGCG derivatives. SH-EP cells with TAMRAAβ42/Aβ42 co-aggregates were treated with 10 μM EGCG or respective EGCG derivatives. Aggregates were quantified after 20 h of incubation from total TAMRA spot intensity per cell and normalized to solvent (DMSO) control. Bars represent mean values ± SD compared to DMSO control from three independent cell culture preparations (n = 3) analyzed in technical triplicates. One-way ANOVA with Dunnett's post hoc test, *$p < 0.05$, **$p < 0.01$, ***$p < 0.001$. (h) Structure of EGCG. Structural elements relevant for cellular Aβ reducing potency are marked in red.
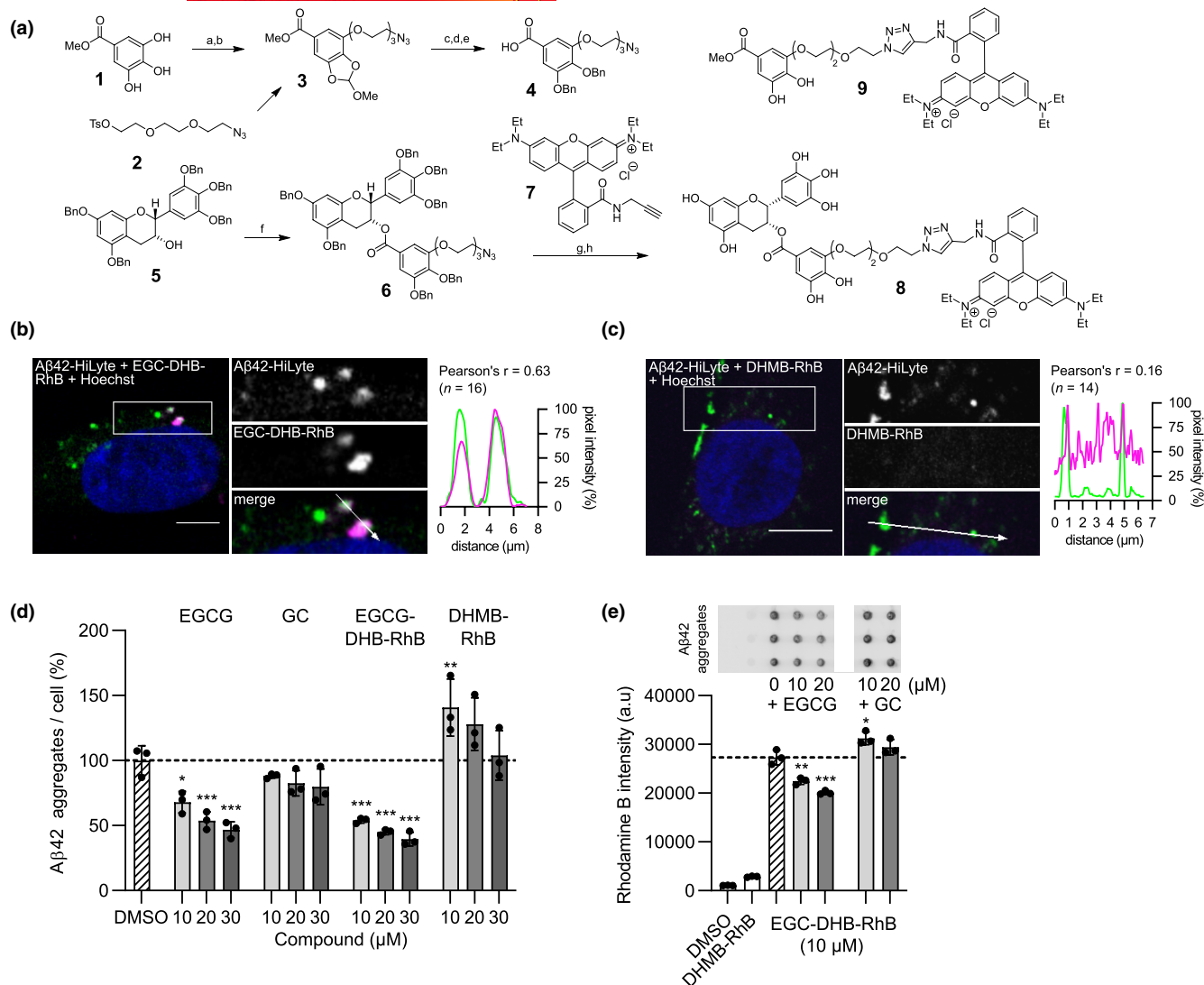
FIGURE 6 The fluorescently labeled EGCG derivative EGC-DHB-Rhodamine directly targets Aβ42 aggregates in cells and in vitro. (a) Chemical synthesis pathway leading to EGC-DHB-Rhodamine: (a) HC(OMe)$_3$, IR-120 plus, toluene, 150 °C, 76%; (b) (2) Cs$_2$CO$_3$, DMF, 78%; (c) p-TsOH, MeOH, 31%; (d) BnCl, K$_2$CO$_3$, DMF, 80 °C, 88%; (e) KOH (40 w%), EtOH, 80 °C, 90%; (f) (4) EDC·HCl, DMAP, CH$_2$Cl$_2$, 84%; (g) CuSO$_4$ (5 mol%), sodium ascorbate (10 mol%), DMSO, 65 °C, 78%; (h) Pd(OH)$_2$, THF/MeOH (1:1), H$_2$ (1 atm), 89% (detailed information, Figure S5). (b,c) SH-EP cells were treated with 1 μM preformed ^{HiLyte}Aβ42/Aβ42 co-aggregates (green puncta) for 4 h. Then, cells were washed, trypsinized, and plated onto glass coverslips. Adherent cells were treated with 20 μM of (B) EGC-DHB-Rhodamine (8) or the rhodamine-labeled control compound (c) DHMB-Rhodamine lacking the catechin moiety (9). After 5 h, cells were fixed, cell nuclei were stained with Hoechst33342 (blue), and confocal imaging was performed. HiLyte (green) and rhodamine B (magenta) fluorescence intensities along white arrows were plotted and Pearson's correlation coefficient (r) was determined for co-localization analysis. Representative regions of interest (ROIs) and co-localization analysis are shown. In total, 16 (b) and 14 (c) ROIs from 12 individual cells for both EGC-DHB-Rhodamine and DHMB-Rhodamine were analyzed resulting in mean Pearson's r of 0.63 and 0.16, respectively. (d) Effects of the compounds EGC-DHB-Rhodamine (EGC-DHB-RhB), EGCG, GC, and DHMB-Rhodamine (DHMB-RhB) on the abundance of preformed ^{HiLyte}Aβ42/Aβ42 co-aggregates in SH-EP cells. EGC-DHB-RhB shows similar activity as EGCG. (e) Binding of EGC-DHB-RhB to preformed Aβ42 aggregates in the presence and absence of EGCG. Aβ42 aggregates (250 ng) were dotted onto nitrocellulose membrane and subsequently incubated with indicated compound concentrations. DMSO or DHMB-RhB show no or weak binding to Aβ42 aggregates. EGC-DHB-RhB shows strong binding to Aβ42 aggregates, which is reduced in the presence of 10 and 20 μM EGCG but not in the presence of GC.

acidification is critical for EGCG-mediated clearance of Aβ42 aggregates in SH-EP cells.

Previous investigations have demonstrated that lysosomal acidification is a prerequisite for the maturation and activation of specific lysosomal proteases (Mauvezin & Neufeld, 2015). Members of the lysosomal cysteine protease family of cathepsins were previously reported to proteolytically cleave Aβ42 (Mueller-Steiner et al., 2006; Suire et al., 2020) and might be involved in the EGCG-induced clearance of intracellular Aβ42 aggregates in SH-EP cells. Therefore, we next analyzed whether inhibition of lysosomal acidification with bafilomycin A1 prevents the maturation of cathepsin B in SH-EP cells. Western blots of SH-EP cell lysates treated with DMSO showed the

cathepsin B proenzyme at ~43 kDa (pro-CatB, Figure 5b) as well as the maturated cathepsin B isoforms at ~27 and ~24 kDa (CatB, Figure 5b). In contrast, samples treated with bafilomycin A1 still showed detectable proenzyme, but almost none of the maturated cathepsin B isoforms (BafA1 pro-CatB & CatB, Figure 5b). Also, the co-treatment of SH-EP cells with bafilomycin A1 and EGCG did not result in effective cathepsin B maturation under these conditions (BafA1 + EGCG, Figure 5b). Next, we analyzed the enzymatic activity of cathepsin B in SH-EP lysates after treatment with bafilomycin A1 alone or with bafilomycin A1 and EGCG. In line with our findings that cathepsin B maturation is decreased upon bafilomycin A1 treatment, we measured a significantly reduced enzymatic activity in bafilomycin A1 treated cells (BafA1 vs. DMSO, Figure 5c). Also, we did not find any change in cathepsin B activity when cells were additionally incubated with EGCG (BafA1 vs. BafA1 + EGCG, Figure 5c), suggesting that both lysosomal acidification and maturation of cathepsin B are critical for EGCG-mediated clearance of preformed intracellular Aβ42 aggregates (− bafilomycin A1, Figure 5a).

We next investigated whether EGCG positively influences cathepsin B maturation in SH-EP cells. Interestingly, we found that the abundance of maturated cathepsin B isoforms was increased in EGCG-treated SH-EP cells (Figure 5d). Furthermore, a concentration-dependent increase in cathepsin B activity was observed (Figure 5e), suggesting that EGCG treatment promotes Aβ42 aggregate degradation in cells because it increases the abundance of active cathepsin B molecules in lysosomes.

Finally, we investigated whether the EGCG-mediated reduction of intracellular Aβ42 aggregates in SH-EP cells is directly linked to the enzymatic activity of lysosomal cathepsins. Since both cathepsin B and L were previously implicated in amyloid degradation and toxicity (Islam et al., 2022; Mueller-Steiner et al., 2006), we assessed the activity of the small molecule inhibitor CA074me (Buttle et al., 1992) in cell-based assays. This compound was previously shown to inhibit both cathepsin B and L in mammalian cells (Montaser et al., 2002). We incubated SH-EP cells containing ᵀᴬᴹᴿᴬAβ42/Aβ42 co-aggregates with 20 μM EGCG and 1, 2.5, 5, and 10 μM CA074me for 20 h and quantified the abundance of TAMRA-labeled Aβ42 co-aggregates by automated microscopy. Interestingly, we observed that inhibition of cathepsin B and L activity with CA074me significantly diminished the EGCG effect on Aβ42 aggregates in a concentration-dependent manner (Figure 5f). This supports our hypothesis that the activity of cathepsin B and/or L is critical for the EGCG-mediated clearance of preformed ᵀᴬᴹᴿᴬAβ42/Aβ42 co-aggregates in SH-EP cells.

3.7 | The fluorescently labeled EGCG derivative EGC-DHB-rhodamine directly targets Aβ42 aggregates in cells and in vitro

EGCG was previously reported to bind preformed Aβ42 aggregates in vitro and to induce their structural remodeling (Bieschke et al., 2010). In addition to the effect of EGCG on the abundance of active cathepsin B isoforms and its enzymatic activity in SH-EP

cells (Figure 5d,e), it might also bind intracellular Aβ42 aggregates and potentially render them more susceptible to cellular degradation. To investigate the association of EGCG with Aβ42 aggregates in SH-EP cells, we synthesized a fluorescently labeled, EGCG-related compound (EGC-DHB-Rhodamine; #8; Figure 6a) that, according to our SAR experiments (Figure 4g), still contains the structural features, which are required for promoting Aβ42 aggregate degradation in cells (Figure 4h). In this compound, the fluorescent tracer dye rhodamine B (#7; Figure 6a), which emits light at 568 nm, is attached via a polyethylene glycol (PEG)-linker to the C3 atom on the 4,5-DHB moiety of EGC-4,5-DHB. In addition, the control compound DHMB-Rhodamine was synthesized (#9; Figure 6a), which lacks the epigallocatechin (EGC) moiety and, therefore, should bind less efficiently to preformed Aβ42 aggregates. Due to the fact that the fluorescent dyes TAMRA and rhodamine B have overlapping emission spectra (Blommel et al., 2004; Sauer et al., 1995), they cannot be applied to monitor the co-localization of ᵀᴬᴹᴿᴬAβ42/Aβ42 co-aggregates and EGC-DHB-Rhodamine in cells. We, therefore, produced additional fibrillar, β-sheet-rich Aβ42 co-aggregates that are labeled with the green fluorescent dye HiLyte Fluor 488 (ᴴⁱᴸʸᵗᵉAβ42/Aβ42 co-aggregates). These structures, similar to ᵀᴬᴹᴿᴬAβ42/Aβ42 co-aggregates, are readily taken up into SH-EP cells (data not shown). However, they appear as green fluorescent puncta in the cytoplasm, when cells are analyzed by fluorescent microscopy (Figure 6b,c). We then treated SH-EP cells harboring ᴴⁱᴸʸᵗᵉAβ42/Aβ42 co-aggregates for 4 h with the chemical compounds EGC-DHB-Rhodamine and DHMB-Rhodamine, respectively, and analyzed their association with the fluorescently labeled aggregates by FM. Strikingly, we found a significant co-localization of EGC-DHB-Rhodamine with ᴴⁱᴸʸᵗᵉAβ42/Aβ42 co-aggregates (Figure 6b), while co-localization between Aβ42 aggregates and the control compound DHMB-Rhodamine was weak (Figure 6c). This indicates that EGC-DHB-Rhodamine directly interacts with the fluorescently labeled Aβ42 co-aggregates in cells.

To investigate whether EGC-DHB-Rhodamine has a similar activity compared to EGCG in promoting the degradation of Aβ42 aggregates in cells, we treated SH-EP cells, which contain ᴴⁱᴸʸᵗᵉAβ42/Aβ42 co-aggregates, with this compound. We found that EGC-DHB-Rhodamine, similarly to EGCG, also significantly reduced the amount of ᴴⁱᴸʸᵗᵉAβ42/Aβ42 co-aggregates in SH-EP cells. In contrast, the non-binding control compound DHMB-Rhodamine, similarly to non-active GC, did not reduce the Aβ42 aggregate load (Figure 6d). Finally, we performed competition experiments to evaluate whether EGC-DHB-Rhodamine and EGCG compete for binding to preformed Aβ42 aggregates in vitro. Aβ42 aggregate preparations (250 ng) dotted onto nitrocellulose membranes were incubated with EGC-DHB-Rhodamine in the absence or presence of different concentrations of EGCG or GC. As a control, Aβ42 aggregates were incubated with DMSO or the control compound DHMB-Rhodamine. Interestingly, in the presence of 10 and 20 μM EGCG, we found significantly reduced binding of EGC-DHB-Rhodamine to preformed Aβ42 aggregates. In comparison, no such effect was observed with the compound GC (Figure 6e). These results indicate that EGC-DHB-Rhodamine and EGCG bind overlapping regions on the surface of Aβ42 aggregates.

Also, they suggest that EGCG similar to EGC-DHB-Rhodamine might directly target preformed Aβ42 aggregates in mammalian cells.

4 | DISCUSSION

The stimulation of protein degradation is an important therapeutic approach, especially in proteinopathies such as AD. Whereas a reduction of the extracellular Aβ plaque load using different Aβ specific antibodies was previously achieved (Panza et al., 2019), this approach has failed to exert profound clinical benefits for AD patients to date (Mullard, 2019). As extracellular Aβ plaque clearance could not efficaciously modulate the disease state, the intracellularly accumulating tau protein and resulting neurofibrillary tangles (NFTs) have gained increasing interest as therapeutic targets in AD. However, especially since it was reported that intracellular Aβ42 aggregates can precede the formation of NFTs and can even stimulate the accumulation of tau proteins (Götz et al., 2001; He et al., 2018; Zempel et al., 2010), intracellular Aβ42 aggregates are also considered to be a promising target. Degradation of specific intracellular proteins, including amyloids, can be achieved using different approaches. PROTACs, hybrid compounds directing target proteins to E3 ligases and the proteasome, can efficiently stimulate protein degradation (Schapira et al., 2019). However, given the poor ability of the proteasome to degrade amyloids, alternative strategies to boost other cellular protein degradation pathways such as autophagy (Siddiqi et al., 2019; Silva et al., 2020), are investigated for amyloid degradation.

To systematically enable the identification of small molecules promoting the degradation of intracellular Aβ42 aggregates, we established a cell-based screening assay. In a focused proof-of-concept screen of a small polyphenol compound library, we identified five small molecules significantly reducing the intracellular Aβ42 aggregate load in SH-EP cells. EGCG, which was previously described to reduce Aβ42 aggregates in cells (Bieschke et al., 2010), most potently stimulated the degradation of intracellular Aβ42 aggregates in a concentration-dependent manner and reduced Aβ42-induced toxicity in SH-EP cells. Interestingly, mechanistic studies revealed that the Aβ42 aggregate degradation-promoting effect is dependent on lysosomal enzyme activity and that cellular inhibition of cathepsins with chemical compounds strongly reduces EGCG-induced Aβ42 aggregate degradation. Cathepsins were previously described to cleave Aβ peptides and were implicated in AD pathogenesis (Sundelöf et al., 2010). However, since cathepsins were shown to cleave APP and thereby might increase Aβ42 production, it was hypothesized that increased cathepsin activity could contribute to disease progression (Hook et al., 2005; Lowry & Klegeris, 2018). This has also led to the evaluation of cathepsin inhibitors in several preclinical AD studies (Hook et al., 2010, 2011). A recent study showed that insufficient lysosomal clearance caused by the knockout of cathepsins can cause neurodegeneration and accumulation of lysosomal bodies in mice (Felbor et al., 2002), which is why a rather protective role of cathepsins in amyloid diseases is implicated (Lambeth et al., 2019). Along this line, it was found that

cathepsin B gene transfer in mice is able to reduce AD-associated phenotypes (Embury et al., 2017; Mueller-Steiner et al., 2006) and that small molecule-mediated upregulation of cathepsin B expression can enhance Aβ42 degradation (Tiribuzi et al., 2017). While enhancing insufficient lysosomal clearance by cathepsin B gene augmentation could be a promising therapeutic approach, small molecules, which increase the abundance of active lysosomal enzymes and thereby increase lysosomal clearance could also be an effective strategy to enhance aggregate clearance. EGCG was previously administered to AD mouse models, where it was shown to reduce extracellular amyloid plaque load (Rezai-Zadeh et al., 2005) and to alleviate cognitive deficits (Bao et al., 2020; Mori et al., 2019). The underlying mechanism for the EGCG-induced reduction of extracellular Aβ plaques, however, is still unclear. It seems feasible to speculate that the increased abundance of active cathepsin B isoforms and their increased enzymatic activity, which we observed upon EGCG treatment in SH-EP cells, could also lead to an enhanced degradation of intracellular Aβ42 aggregates in vivo.

Another potential mechanism that might lead to EGCG-mediated Aβ42 aggregate degradation in cells, could involve its previously described activity to remodel fibrillar Aβ aggregates into amorphous substructures (Ehrnhoefer et al., 2008). Such Aβ42 and α-synuclein oligomers that are generated in the presence of EGCG in vitro have been shown to be less toxic for cells than fibrillar Aβ42 aggregates (Bieschke et al., 2010). Whether these EGCG-induced oligomers show differential uptake and/or processing within microglia, astrocytes, or macrophages compared to fibrillar Aβ aggregates, is unknown. Interestingly, EGCG was recently reported to induce conformational changes in amyloid fibrils consisting of the transforming growth factor-β-induced protein (TGFBIp) in lattice corneal dystrophy. These structural changes facilitated the proteolytic cleavage of TGFBIp by proteinase K (Stenvang et al., 2016). EGCG could act in a similar way on intracellular Aβ42 aggregates. Previous studies showed that internalized Aβ42 aggregates accumulating in late endosomes and lysosomes are largely resistant to degradation (Burdick et al., 1997; Knauer et al., 1992; Morelli et al., 1999; Morishima-Kawashima & Ihara, 1998). Thus, direct binding of EGCG to intracellular Aβ42 aggregates could render them more susceptible to lysosomal degradation. To evaluate whether EGCG is in fact able to directly bind to intracellular Aβ42 aggregates, we synthesized a novel fluorescently labeled EGCG derivative, which still contains the structural moieties that are relevant for the Aβ42 aggregate reducing effect in cells (Figure 4g). We found this EGCG derivative to co-localize with Aβ42 aggregates in cells, whereas a fluorescently labeled control compound lacking the catechin moiety, showed no co-localization with Aβ42 aggregates. Importantly, this novel EGCG derivative also stimulates the degradation of Aβ42 aggregates in cells and binds competitively with EGCG to preformed Aβ42 aggregates in vitro. While this is no direct evidence for the intracellular remodeling of Aβ42 aggregates into specific degradable subspecies, binding of EGCG to intracellular Aβ42 aggregates could indicate that it potentially renders them more susceptible to degradation.

Previously, it was demonstrated that EGCG directly interacts with multiple human proteins (Lorenz, 2013; Negri et al., 2018; Zhao et al., 2021), suggesting that its cellular activity results from activating and/or repressing a wide range of complex biological processes and pathways. Our study suggests that EGCG promotes the degradation of preformed, fibrillar Aβ42 aggregates in neuroblastoma cells by increasing the lysosomal activities of cathepsins. In addition, our results indicate that it directly targets amyloidogenic protein aggregates in cells and potentially facilitates their structural remodeling in vivo. Since EGCG is reported to have polypharmacological activities in cells, additional mechanisms leading to the observed effects are certainly possible. Thus, further investigations will be needed to comprehensively understand the mechanism of action of EGCG in cells.

AUTHOR CONTRIBUTIONS

ACKNOWLEDGMENTS

CONFLICT OF INTEREST STATEMENT

The authors declare no conflict of interest.

DATA AVAILABILITY STATEMENT

Data available on request from the authors.

ORCID

Christopher Secker https://orcid.org/0000-0002-7222-536X

Erich E. Wanker https://orcid.org/0000-0001-8072-1630

REFERENCES

Bao, J., Liu, W., Zhou, H. Y., Gui, Y. R., Yang, Y. H., Wu, M. J., Xiao, Y. F., Shang, J. T., Long, G. F., & Shu, X. J. (2020). Epigallocatechin-3-gallate alleviates cognitive deficits in APP/PS1 mice. *Current Medical Science*, 40, 18–27.

Baumketner, A., Bernstein, S. L., Wyttenbach, T., Bitan, G., Teplow, D. B., Bowers, M. T., & Shea, J. E. (2006). Amyloid beta-protein monomer structure: A computational and experimental study. *Protein Science*, 15, 420–428.

Benilova, I., Karran, E., & De Strooper, B. (2012). The toxic Aβ oligomer and Alzheimer's disease: An emperor in need of clothes. *Nature Neuroscience*, 15, 349–357.

Biancalana, M., & Koide, S. (2010). Molecular mechanism of Thioflavin-T binding to amyloid fibrils. *Biochimica et Biophysica Acta*, 1804, 1405–1412.

Bickel, P. E., Scherer, P. E., Schnitzer, J. E., Oh, P., Lisanti, M. P., & Lodish, H. F. (1997). Flotillin and epidermal surface antigen define a new family of caveolae-associated integral membrane proteins. *The Journal of Biological Chemistry*, 272, 13793–13802.

Bieschke, J., Russ, J., Friedrich, R. P., Ehrnhoefer, D. E., Wobst, H., Neugebauer, K., & Wanker, E. E. (2010). EGCG remodels mature alpha-synuclein and amyloid-beta fibrils and reduces cellular toxicity. *Proceedings of the National Academy of Sciences of the United States of America*, 107, 7710–7715.

Blommel, P., Hanson, G. T., & Vogel, K. W. (2004). Multiplexing fluorescence polarization assays to increase information content per screen: Applications for screening steroid hormone receptors. *Journal of Biomolecular Screening*, 9, 294–302.

Boeddrich, A., Babila, J. T., Wiglenda, T., Diez, L., Jacob, M., Nietfeld, W., Huska, M. R., Haenig, C., Groenke, N., Buntru, A., Blanc, E., Meier, J. C., Vannoni, E., Erck, C., Friedrich, B., Martens, H., Neuendorf, N., Schnoegl, S., Wolfer, D. P., ... Wanker, E. E. (2019). The anti-amyloid compound DO1 decreases plaque pathology and neuroinflammation-related expression changes in 5xFAD transgenic mice. *Cell Chemical Biology*, 26, 109–120.e7.

Bondeson, D. P., Mares, A., Smith, I. E. D., Ko, E., Campos, S., Miah, A. H., Mulholland, K. E., Routly, N., Buckley, D. L., Gustafson, J. L., Zinn, N., Grandi, P., Shimamura, S., Bergamini, G., Faelth-Savitski, M., Bantscheff, M., Cox, C., Gordon, D. A., Willard, R. R., ... Crews, C. M. (2015). Catalytic in vivo protein knockdown by small-molecule PROTACs. *Nature Chemical Biology*, 11, 611–617.

Bückig, A., Tikkanen, R., Herzog, V., & Schmitz, A. (2002). Cytosolic and nuclear aggregation of the amyloid beta-peptide following its expression in the endoplasmic reticulum. *Histochemistry and Cell Biology*, 118, 353–360.

Burdick, D., Kosmoski, J., Knauer, M. F., & Glabe, C. G. (1997). Preferential adsorption, internalization and resistance to degradation of the major isoform of the Alzheimer's amyloid peptide, A beta 1-42, in differentiated PC12 cells. *Brain Research*, 746, 275–284.

Buttle, D. J., Murata, M., Knight, C. G., & Barrett, A. J. (1992). CA074 methyl ester: A proinhibitor for intracellular cathepsin B. *Archives of Biochemistry and Biophysics*, 299, 377–380.

Carson, C. (2012). The effective use of effect size indices in institutional research. In *31st Annual conference proceedings* (Vol. 41). NEAIR.

Castellani, R. J., Lee, H. G., Zhu, X., Nunomura, A., Perry, G., & Smith, M. A. (2006). Neuropathology of Alzheimer disease:

Pathognomonic but not pathogenic. *Acta Neuropathologica*, 111, 503–509.

Chen, J. W., Murphy, T. L., Willingham, M. C., Pastan, I., & August, J. T. (1985). Identification of two lysosomal membrane glycoproteins. *The Journal of Cell Biology*, 101, 85–95.

Chen, Z.-Y., Zhu, Q. Y., Wong, Y. F., Zhang, Z., & Chung, H. Y. (1998). Stabilizing effect of ascorbic acid on green tea catechins. *Journal of Agricultural and Food Chemistry*, 46, 2512–2516.

Chiti, F., & Dobson, C. M. (2017). Protein misfolding, amyloid formation, and human disease: A summary of progress over the last decade. *Annual Review of Biochemistry*, 86, 27–68.

Costes, S. V., Daelemans, D., Cho, E. H., Dobbin, Z., Pavlakis, G., & Lockett, S. (2004). Automatic and quantitative measurement of protein-protein colocalization in live cells. *Biophysical Journal*, 86, 3993–4003.

Ehrnhoefer, D. E., Bieschke, J., Boeddrich, A., Herbst, M., Masino, L., Lurz, R., Engemann, S., Pastore, A., & Wanker, E. E. (2008). EGCG redirects amyloidogenic polypeptides into unstructured, off-pathway oligomers. *Nature Structural & Molecular Biology*, 15, 558–566.

Ehrnhoefer, D. E., Duennwald, M., Markovic, P., Wacker, J. L., Engemann, S., Roark, M., Legleiter, J., Marsh, J. L., Thompson, L. M., Lindquist, S., Muchowski, P. J., & Wanker, E. E. (2006). Green tea (–)-epigallocatechin-gallate modulates early events in huntingtin misfolding and reduces toxicity in Huntington's disease models. *Human Molecular Genetics*, 15, 2743–2751.

Embury, C. M., Dyavarshetty, B., Lu, Y., Wiederin, J. L., Ciborowski, P., Gendelman, H. E., & Kiyota, T. (2017). Cathepsin B improves β-amyloidosis and learning and memory in models of Alzheimer's disease. *Journal of Neuroimmune Pharmacology*, 12, 340–352.

Engel, M. F. M., Khemtémourian, L., Kleijer, C. C., Meeldijk, H. J. D., Jacobs, J., Verkleij, A. J., de Kruijff, B., Killian, J. A., & Höppener, J. W. M. (2008). Membrane damage by human islet amyloid polypeptide through fibril growth at the membrane. *Proceedings of the National Academy of Sciences of the United States of America*, 105, 6033–6038.

Eskelinen, E.-L., Illert, A. L., Tanaka, Y., Schwarzmann, G., Blanz, J., von Figura, K., & Saftig, P. (2002). Role of LAMP-2 in lysosome biogenesis and autophagy. *Molecular Biology of the Cell*, 13, 3355–3368.

Felbor, U., Kessler, B., Mothes, W., Goebel, H. H., Ploegh, H. L., Bronson, R. T., & Olsen, B. R. (2002). Neuronal loss and brain atrophy in mice lacking cathepsins B and L. *Proceedings of the National Academy of Sciences of the United States of America*, 99, 7883–7888.

Foley, A. R., Roseman, G. P., Chan, K., Smart, A., Finn, T. S., Yang, K., Lokey, R. S., Millhauser, G. L., & Raskatov, J. A. (2020). Evidence for aggregation-independent, PrPC-mediated Aβ cellular internalization. *Proceedings of the National Academy of Sciences of the United States of America*, 117, 28625–28631.

Gazova, Z., Siposova, K., Kurin, E., Mučaji, P., & Nagy, M. (2013). Amyloid aggregation of lysozyme: The synergy study of red wine polyphenols. *Proteins*, 81, 994–1004.

Götz, J., Chen, F., van Dorpe, J., & Nitsch, R. M. (2001). Formation of neurofibrillary tangles in P301l tau transgenic mice induced by Abeta 42 fibrils. *Science*, 293, 1491–1495.

Gremer, L., Schölzel, D., Schenk, C., Reinartz, E., Labahn, J., Ravelli, R. B. G., Tusche, M., Lopez-Iglesias, C., Hoyer, W., Heise, H., Willbold, D., & Schröder, G. F. (2017). Fibril structure of amyloid-β(1-42) by cryo-electron microscopy. *Science*, 358, 116–119.

Groenning, M. (2009). Binding mode of Thioflavin T and other molecular probes in the context of amyloid fibrils—Current status. *Journal of Chemical Biology*, 3, 1–18.

Gyure, K. A., Durham, R., Stewart, W. F., Smialek, J. E., & Troncoso, J. C. (2001). Intraneuronal abeta-amyloid precedes development of amyloid plaques in Down syndrome. *Archives of Pathology & Laboratory Medicine*, 125, 489–492.

Haney, C. M., Cleveland, C. L., Wissner, R. F., Owei, L., Robustelli, J., Daniels, M. J., Canyurt, M., Rodriguez, P., Ischiropoulos, H., Baumgart, T., & Petersson, E. J. (2017). Site-specific fluorescence polarization for studying the disaggregation of α-synuclein fibrils by small molecules. *Biochemistry*, 56, 683–691.

Hatami, A., Albay, R., Monjazeb, S., Milton, S., & Glabe, C. (2014). Monoclonal antibodies against Aβ42 fibrils distinguish multiple aggregation state polymorphisms in vitro and in alzheimer disease brain. *The Journal of Biological Chemistry*, 289, 32131–32143.

Hatami, A., Monjazeb, S., & Glabe, C. (2016). The anti-amyloid-β monoclonal antibody 4G8 recognizes a generic sequence-independent epitope associated with α-synuclein and islet amyloid polypeptide amyloid fibrils. *Journal of Alzheimer's Disease*, 50, 517–525.

Hayashi, N., & Ujihara, T. (2017). Conformations of flavan-3-ols in water: Analysis using density functional theory. *Journal of Natural Products*, 80, 319–327.

He, Z., Guo, J. L., McBride, J. D., Narasimhan, S., Kim, H., Changolkar, L., Zhang, B., Gathagan, R. J., Yue, C., Dengler, C., Stieber, A., Nitla, M., Coulter, D. A., Abel, T., Brunden, K. R., Trojanowski, J. Q., & Lee, V. M. Y. (2018). Amyloid-β plaques enhance Alzheimer's brain tau-seeded pathologies by facilitating neuritic plaque tau aggregation. *Nature Medicine*, 24, 29–38.

Hook, G., Hook, V., & Kindy, M. (2011). The cysteine protease inhibitor, E64d, reduces brain amyloid-β and improves memory deficits in Alzheimer's disease animal models by inhibiting cathepsin B, but not BACE1, β-secretase activity. *Journal of Alzheimer's Disease*, 26, 387–408.

Hook, V., Hook, G., & Kindy, M. (2010). Pharmacogenetic features of cathepsin B inhibitors that improve memory deficit and reduce beta-amyloid related to Alzheimer's disease. *Biological Chemistry*, 391, 861–872.

Hook, V., Toneff, T., Bogyo, M., Greenbaum, D., Medzihradszky, K. F., Neveu, J., Lane, W., Hook, G., & Reisine, T. (2005). Inhibition of cathepsin B reduces beta-amyloid production in regulated secretory vesicles of neuronal chromaffin cells: Evidence for cathepsin B as a candidate beta-secretase of Alzheimer's disease. *Biological Chemistry*, 386, 931–940.

Huang, L., McClatchy, D. B., Maher, P., Liang, Z., Diedrich, J. K., Soriano-Castell, D., Goldberg, J., Shokhirev, M., Yates, J. R., III, Schubert, D., & Currais, A. (2020). Intracellular amyloid toxicity induces oxytosis/ferroptosis regulated cell death. *Cell Death & Disease*, 11, 828.

Ishizu, T., Tsutsumi, H., Yamamoto, H., & Harano, K. (2009). NMR spectroscopic characterization of inclusion complexes comprising cyclodextrins and gallated catechins in aqueous solution: Cavity size dependency. *Magnetic Resonance in Chemistry*, 47, 283–287.

Islam, M. I., Nagakannan, P., Shcholok, T., Contu, F., Mai, S., Albensi, B. C., del Bigio, M. R., Wang, J. F., Sharoar, M. G., Yan, R., Park, I. S., & Eftekharpour, E. (2022). Regulatory role of cathepsin L in induction of nuclear laminopathy in Alzheimer's disease. *Aging Cell*, 21, e13531.

Kada, T., Kaneko, K., Matsuzaki, S., Matsuzaki, T., & Hara, Y. (1985). Detection and chemical identification of natural bio-antimutagens. A case of the green tea factor. *Mutation Research*, 150, 127–132.

Kelényi, G. (1967). Thioflavin S fluorescent and Congo red anisotropic stainings in the histologic demonstration of amyloid. *Acta Neuropathologica*, 7, 336–348.

Kim, Y. E., Hosp, F., Frottin, F., Ge, H., Mann, M., Hayer-Hartl, M., & Hartl, F. U. (2016). Soluble oligomers of PolyQ-expanded huntingtin target a multiplicity of key cellular factors. *Molecular Cell*, 63, 951–964.

Knauer, M. F., Soreghan, B., Burdick, D., Kosmoski, J., & Glabe, C. G. (1992). Intracellular accumulation and resistance to degradation of the Alzheimer amyloid A4/beta protein. *Proceedings of the National Academy of Sciences of the United States of America*, 89, 7437–7441.

Knopman, D. S., Amieva, H., Petersen, R. C., Chételat, G., Holtzman, D. M., Hyman, B. T., Nixon, R. A., & Jones, D. T. (2021). Alzheimer disease. *Nature Reviews Disease Primers*, 7, 33.

Kollmer, M., Close, W., Funk, L., Rasmussen, J., Bsoul, A., Schierhorn, A., Schmidt, M., Sigurdson, C. J., Jucker, M., & Fändrich, M. (2019).

Cryo-EM structure and polymorphism of Aβ amyloid fibrils purified from Alzheimer's brain tissue. *Nature Communications*, 10, 4760.

Konar, M., Ghosh, D., Samanta, S., & Govindaraju, T. (2022). Combating amyloid-induced cellular toxicity and stiffness by designer peptidomimetics. *RSC Chemical Biology*, 3, 220–226.

Krohn, K., Ahmed, I., & John, M. (2009). Enantioselective synthesis of flavan-3-ols using a mitsunobu cyclization. *Synthesis*, 2009, 779–786.

Ladiwala, A. R. A., Lin, J. C., Bale, S. S., Marcelino-Cruz, A. M., Bhattacharya, M., Dordick, J. S., & Tessier, P. M. (2010). Resveratrol selectively remodels soluble oligomers and fibrils of amyloid Abeta into off-pathway conformers. *The Journal of Biological Chemistry*, 285, 24228–24237.

LaFerla, F. M., Green, K. N., & Oddo, S. (2007). Intracellular amyloid-beta in Alzheimer's disease. *Nature Reviews Neuroscience*, 8, 499–509.

Lai, A. Y., & McLaurin, J. (2010). Mechanisms of amyloid-beta peptide uptake by neurons: The role of lipid rafts and lipid raft-associated proteins. *International Journal of Alzheimer's Disease*, 2011, e548380.

Lambeth, T. R., Riggs, D. L., Talbert, L. E., Tang, J., Coburn, E., Kang, A. S., Noll, J., Augello, C., Ford, B. D., & Julian, R. R. (2019). Spontaneous isomerization of long-lived proteins provides a molecular mechanism for the lysosomal failure observed in Alzheimer's disease. *ACS Central Science*, 5, 1387–1395.

Lee, J.-H., Yang, D. S., Goulbourne, C. N., Im, E., Stavrides, P., Pensalfini, A., Chan, H., Bouchet-Marquis, C., Bleiwas, C., Berg, M. J., Huo, C., Peddy, J., Pawlik, M., Levy, E., Rao, M., Staufenbiel, M., & Nixon, R. A. (2022). Faulty autolysosome acidification in Alzheimer's disease mouse models induces autophagic build-up of Aβ in neurons, yielding senile plaques. *Nature Neuroscience*, 25, 688–701.

Leeman, D. S., Hebestreit, K., Ruetz, T., Webb, A. E., McKay, A., Pollina, E. A., Dulken, B. W., Zhao, X., Yeo, R. W., Ho, T. T., Mahmoudi, S., Devarajan, K., Passegué, E., Rando, T. A., Frydman, J., & Brunet, A. (2018). Lysosome activation clears aggregates and enhances quiescent neural stem cell activation during aging. *Science*, 359, 1277–1283.

Liberal, J., Francisco, V., Costa, G., Figueirinha, A., Amaral, M. T., Marques, C., Girão, H., Lopes, M. C., Cruz, M. T., & Batista, M. T. (2014). Bioactivity of Fragaria vesca leaves through inflammation, proteasome and autophagy modulation. *Journal of Ethnopharmacology*, 158, 113–122.

Lorenz, M. (2013). Cellular targets for the beneficial actions of tea polyphenols. *The American Journal of Clinical Nutrition*, 98, 1642S–1650S.

Lowry, J. R., & Klegeris, A. (2018). Emerging roles of microglial cathepsins in neurodegenerative disease. *Brain Research Bulletin*, 139, 144–156.

Lu, K., den Brave, F., & Jentsch, S. (2017). Receptor oligomerization guides pathway choice between proteasomal and autophagic degradation. *Nature Cell Biology*, 19, 732–739.

Lu, P., Liu, J., & Koestler, D. (2017). pwr2: Power and sample size analysis for one-way and two-way ANOVA models. https://cran.r-project.org/web/packages/pwr2/pwr2.pdf

Marshall, K. E., Vadukul, D. M., Staras, K., & Serpell, L. C. (2020). Misfolded amyloid-β-42 impairs the endosomal-lysosomal pathway. *Cellular and Molecular Life Sciences*, 77, 5031–5043.

Matos, A. M., Cristóvão, J. S., Yashunsky, D. V., Nifantiev, N. E., Viana, A. S., Gomes, C. M., & Rauter, A. P. (2017). Synthesis and effects of flavonoid structure variation on amyloid-β aggregation. *Pure and Applied Chemistry*, 89, 1305–1320.

Mauvezin, C., & Neufeld, T. P. (2015). Bafilomycin A1 disrupts autophagic flux by inhibiting both V-ATPase-dependent acidification and Ca-P60A/SERCA-dependent autophagosome-lysosome fusion. *Autophagy*, 11, 1437–1438.

May, J. A., Ratan, H., Glenn, J. R., Losche, W., Spangenberg, P., & Heptinstall, S. (1998). GPIIb-IIIa antagonists cause rapid disaggregation of platelets pre-treated with cytochalasin D. Evidence that the stability of platelet aggregates depends on normal cytoskeletal assembly. *Platelets*, 9, 227–232.

Mindell, J. A. (2012). Lysosomal acidification mechanisms. *Annual Review of Physiology*, 74, 69–86.

Modernelli, A., Naponelli, V., Giovanna Troglio, M., Bonacini, M., Ramazzina, I., Bettuzzi, S., & Rizzi, F. (2015). EGCG antagonizes bortezomib cytotoxicity in prostate cancer cells by an autophagic mechanism. *Scientific Reports*, 5, 15270.

Montaser, M., Lalmanach, G., & Mach, L. (2002). CA-074, but not its methyl ester CA-074Me, is a selective inhibitor of cathepsin B within living cells. *Biological Chemistry*, 383, 1305–1308.

Morelli, L., Giambartolomei, G. H., Prat, M. I., & Castaño, E. M. (1999). Internalization and resistance to degradation of Alzheimer's A beta 1-42 at nanomolar concentrations in THP-1 human monocytic cell line. *Neuroscience Letters*, 262, 5–8.

Mori, T., Koyama, N., Tan, J., Segawa, T., Maeda, M., & Town, T. (2019). Combined treatment with the phenolics (−)-epigallocatechin-3-gallate and ferulic acid improves cognition and reduces Alzheimer-like pathology in mice. *The Journal of Biological Chemistry*, 294, 2714–5444.

Morishima-Kawashima, M., & Ihara, Y. (1998). The presence of amyloid beta-protein in the detergent-insoluble membrane compartment of human neuroblastoma cells. *Biochemistry*, 37, 15247–15253.

Mueller-Steiner, S., Zhou, Y., Arai, H., Roberson, E. D., Sun, B., Chen, J., Wang, X., Yu, G., Esposito, L., Mucke, L., & Gan, L. (2006). Antiamyloidogenic and neuroprotective functions of cathepsin B: Implications for Alzheimer's disease. *Neuron*, 51, 703–714.

Mullard, A. (2019). Anti-amyloid failures stack up as Alzheimer antibody flops. *Nature Reviews Drug Discovery*, 18, 327. https://doi.org/10.1038/d41573-019-00064-1

Naiki, H., Higuchi, K., Hosokawa, M., & Takeda, T. (1989). Fluorometric determination of amyloid fibrils in vitro using the fluorescent dye, thioflavin T1. *Analytical Biochemistry*, 177, 244–249.

Negri, A., Naponelli, V., Rizzi, F., & Bettuzzi, S. (2018). Molecular targets of epigallocatechin—Gallate (EGCG): A special focus on signal transduction and cancer. *Nutrients*, 10, 1936.

Nichols, M. R., Moss, M. A., Reed, D. K., Cratic-McDaniel, S., Hoh, J. H., & Rosenberry, T. L. (2005). Amyloid-β protofibrils differ from amyloid-β aggregates induced in dilute hexafluoroisopropanol in stability and morphology. *The Journal of Biological Chemistry*, 280, 2471–2480.

Nicoll, A. J., Panico, S., Freir, D. B., Wright, D., Terry, C., Risse, E., Herron, C. E., O'Malley, T., Wadsworth, J. D. F., Farrow, M. A., Walsh, D. M., Saibil, H. R., & Collinge, J. (2013). Amyloid-β nanotubes are associated with prion protein-dependent synaptotoxicity. *Nature Communications*, 4, 2416.

Oddo, S., Caccamo, A., Smith, I. F., Green, K. N., & LaFerla, F. M. (2006). A dynamic relationship between intracellular and extracellular pools of Abeta. *The American Journal of Pathology*, 168, 184–194.

Ono, K., Yoshiike, Y., Takashima, A., Hasegawa, K., Naiki, H., & Yamada, M. (2003). Potent anti-amyloidogenic and fibril-destabilizing effects of polyphenols in vitro: Implications for the prevention and therapeutics of Alzheimer's disease. *Journal of Neurochemistry*, 87, 172–181.

Palhano, F. L., Lee, J., Grimster, N. P., & Kelly, J. W. (2013). Toward the molecular mechanism(s) by which EGCG treatment remodels mature amyloid fibrils. *Journal of the American Chemical Society*, 135, 7503–7510.

Panza, F., Lozupone, M., Logroscino, G., & Imbimbo, B. P. (2019). A critical appraisal of amyloid-β-targeting therapies for Alzheimer disease. *Nature Reviews Neurology*, 15, 73–88.

Pieri, L., Madiona, K., Bousset, L., & Melki, R. (2012). Fibrillar α-synuclein and huntingtin exon 1 assemblies are toxic to the cells. *Biophysical Journal*, 102, 2894–2905.

Proniuk, S., Liederer, B. M., & Blanchard, J. (2002). Preformulation study of epigallocatechin gallate, a promising antioxidant for topical skin cancer prevention. *Journal of Pharmaceutical Sciences*, 91, 111–116.

Regitz, C., Dußling, L. M., & Wenzel, U. (2014). Amyloid-beta (Aβ$_{1-42}$)-induced paralysis in Caenorhabditis elegans is inhibited by the

polyphenol quercetin through activation of protein degradation pathways. *Molecular Nutrition & Food Research*, 58, 1931–1940.

Rezai-Zadeh, K., Shytle, D., Sun, N., Mori, T., Hou, H., Jeanniton, D., Ehrhart, J., Townsend, K., Zeng, J., Morgan, D., Hardy, J., Town, T., & Tan, J. (2005). Green tea epigallocatechin-3-gallate (EGCG) modulates amyloid precursor protein cleavage and reduces cerebral amyloidosis in alzheimer transgenic mice. *The Journal of Neuroscience*, 25, 8807–8814.

Ripoli, C., Cocco, S., Li Puma, D. D., Piacentini, R., Mastrodonato, A., Scala, F., Puzzo, D., D'Ascenzo, M., & Grassi, C. (2014). Intracellular accumulation of amyloid-β (Aβ) protein plays a major role in Aβ-induced alterations of glutamatergic synaptic transmission and plasticity. *Journal of Neuroscience*, 34, 12893–12903.

Sauer, M., Han, K. T., Müller, R., Nord, S., Schulz, A., Seeger, S., Wolfrum, J., Arden-Jacob, J., Deltau, G., Marx, N. J., Zander, C., & Drexhage, K. H. (1995). New fluorescent dyes in the red region for biodiagnostics. *Journal of Fluorescence*, 5, 247–261.

Schapira, M., Calabrese, M. F., Bullock, A. N., & Crews, C. M. (2019). Targeted protein degradation: Expanding the toolbox. *Nature Reviews Drug Discovery*, 18, 949–963.

Schmidt, M., Sachse, C., Richter, W., Xu, C., Fändrich, M., & Grigorieff, N. (2009). Comparison of Alzheimer Abeta(1-40) and Abeta(1-42) amyloid fibrils reveals similar protofilament structures. *Proceedings of the National Academy of Sciences of the United States of America*, 106, 19813–19818.

Schneekloth, A. R., Pucheault, M., Tae, H. S., & Crews, C. M. (2008). Targeted intracellular protein degradation induced by a small molecule: En route to chemical proteomics. *Bioorganic & Medicinal Chemistry Letters*, 18, 5904–5908.

Sharoar, M. G., Thapa, A., Shahnawaz, M., Ramasamy, V. S., Woo, E. R., Shin, S. Y., & Park, I. S. (2012). Keampferol-3-O-rhamnoside abrogates amyloid beta toxicity by modulating monomers and remodeling oligomers and fibrils to non-toxic aggregates. *Journal of Biomedical Science*, 19, 104.

Shiba, A., Kinoshita-Kikuta, E., Kinoshita, E., & Koike, T. (2017). TAMRA/TAMRA fluorescence quenching systems for the activity assay of alkaline phosphatase. *Sensors*, 17(8), 187.

Siddiqi, F. H., Menzies, F. M., Lopez, A., Stamatakou, E., Karabiyik, C., Ureshino, R., Ricketts, T., Jimenez-Sanchez, M., Esteban, M. A., Lai, L., Tortorella, M. D., Luo, Z., Liu, H., Metzakopian, E., Fernandes, H. J. R., Bassett, A., Karran, E., Miller, B. L., Fleming, A., & Rubinsztein, D. C. (2019). Felodipine induces autophagy in mouse brains with pharmacokinetics amenable to repurposing. *Nature Communications*, 10, 1817.

Silva, M. C., Nandi, G. A., Tentarelli, S., Gurrell, I. K., Jamier, T., Lucente, D., Dickerson, B. C., Brown, D. G., Brandon, N. J., & Haggarty, S. J. (2020). Prolonged tau clearance and stress vulnerability rescue by pharmacological activation of autophagy in tauopathy neurons. *Nature Communications*, 11, 3258.

Sloane, J. A., Pietropaolo, M. F., Rosene, D. L., Moss, M. B., Peters, A., Kemper, T., & Abraham, C. R. (1997). Lack of correlation between plaque burden and cognition in the aged monkey. *Acta Neuropathologica*, 94, 471–478.

Sowade, R. F., & Jahn, T. R. (2017). Seed-induced acceleration of amyloid-β mediated neurotoxicity in vivo. *Nature Communications*, 8, 512.

Stenvang, M., Christiansen, G., & Otzen, D. E. (2016). Epigallocatechin gallate remodels fibrils of lattice corneal dystrophy protein, facilitating proteolytic degradation and preventing formation of membrane-permeabilizing species. *Biochemistry*, 55, 2344–2357.

Sternke-Hoffmann, R., Peduzzo, A., Bolakhrif, N., Haas, R., & Buell, A. K. (2020). The aggregation conditions define whether EGCG is an inhibitor or enhancer of α-synuclein amyloid fibril formation. *International Journal of Molecular Sciences*, 21, 1995.

Stroud, J. C., Liu, C., Teng, P. K., & Eisenberg, D. (2012). Toxic fibrillar oligomers of amyloid-β have cross-β structure. *Proceedings of the National Academy of Sciences of the United States of America*, 109, 7717–7722.

Suire, C. N., Abdul-Hay, S. O., Sahara, T., Kang, D., Brizuela, M. K., Saftig, P., Dickson, D. W., Rosenberry, T. L., & Leissring, M. A. (2020). Cathepsin D regulates cerebral Aβ42/40 ratios via differential degradation of Aβ42 and Aβ40. *Alzheimer's Research & Therapy*, 12, 80.

Sullivan, G. M., & Feinn, R. (2012). Using effect size—Or why the p value is not enough. *Journal of Graduate Medical Education*, 4, 279–282.

Sundelöf, J., Sundström, J., Hansson, O., Eriksdotter-Jönhagen, M., Giedraitis, V., Larsson, A., Degerman-Gunnarsson, M., Ingelsson, M., Minthon, L., Blennow, K., Kilander, L., Basun, H., & Lannfelt, L. (2010). Higher cathepsin B levels in plasma in Alzheimer's disease compared to healthy controls. *Journal of Alzheimer's Disease*, 22, 1223–1230.

Takahashi, R. H., Nagao, T., & Gouras, G. K. (2017). Plaque formation and the intraneuronal accumulation of β-amyloid in Alzheimer's disease. *Pathology International*, 67, 185–193.

Thal, D. R., Walter, J., Saido, T. C., & Fändrich, M. (2015). Neuropathology and biochemistry of Aβ and its aggregates in Alzheimer's disease. *Acta Neuropathologica*, 129, 167–182.

Tipping, K. W., van Oosten-Hawle, P., Hewitt, E. W., & Radford, S. E. (2015). Amyloid fibres: Inert end-stage aggregates or key players in disease? *Trends in Biochemical Sciences*, 40, 719–727.

Tiribuzi, R., Crispoltoni, L., Chiurchiù, V., Casella, A., Montecchiani, C., del Pino, A. M., Maccarrone, M., Palmerini, C. A., Caltagirone, C., Kawarai, T., Orlacchio, A., & Orlacchio, A. (2017). Trans-crocetin improves amyloid-β degradation in monocytes from Alzheimer's disease patients. *Journal of the Neurological Sciences*, 372, 408–412.

Vadukul, D. M., Maina, M., Franklin, H., Nardecchia, A., Serpell, L. C., & Marshall, K. E. (2020). Internalisation and toxicity of amyloid-β 1-42 are influenced by its conformation and assembly state rather than size. *FEBS Letters*, 594, 3490–3503.

Velander, P., Wu, L., Henderson, F., Zhang, S., Bevan, D. R., & Xu, B. (2017). Natural product-based amyloid inhibitors. *Biochemical Pharmacology*, 139, 40–55.

Volpicelli-Daley, L. A., Luk, K. C., Patel, T. P., Tanik, S. A., Riddle, D. M., Stieber, A., Meaney, D. F., Trojanowski, J. Q., & Lee, V. M. Y. (2011). Exogenous α-synuclein fibrils induce Lewy body pathology leading to synaptic dysfunction and neuron death. *Neuron*, 72, 57–71.

Wanker, E. E., Scherzinger, E., Heiser, V., Sittler, A., Eickhoff, H., & Lehrach, H. (1999). Membrane filter assay for detection of amyloid-like polyglutamine-containing protein aggregates. *Methods in Enzymology*, 309, 375–386.

Wirths, O., Multhaup, G., Czech, C., Blanchard, V., Moussaoui, S., Tremp, G., Pradier, L., Beyreuther, K., & Bayer, T. A. (2001). Intraneuronal Abeta accumulation precedes plaque formation in beta-amyloid precursor protein and presenilin-1 double-transgenic mice. *Neuroscience Letters*, 306, 116–120.

Wood, E. (1994). Molecular probes: Handbook of fluorescent probes and research chemicals: By R P Haugland. pp 390. Interchim (Molecular Probes Inc, PO Box 22010 Eugene, OR 97402-0414, USA, or 15 rue des Champs, 92600 Asnieres, Paris). 1992–1994. $15. *Biochemical Education*, 22, 83.

Yeh, F. L., Wang, Y., Tom, I., Gonzalez, L. C., & Sheng, M. (2016). TREM2 binds to apolipoproteins, including APOE and CLU/APOJ, and thereby facilitates uptake of amyloid-beta by microglia. *Neuron*, 91, 328–340.

Zeineddine, R., & Yerbury, J. J. (2015). The role of macropinocytosis in the propagation of protein aggregation associated with neurodegenerative diseases. *Frontiers in Physiology*, 6, 277. https://doi.org/10.3389/fphys.2015.00277/full

Zempel, H., Thies, E., Mandelkow, E., & Mandelkow, E.-M. (2010). Abeta oligomers cause localized Ca(2+) elevation, missorting of

endogenous Tau into dendrites, Tau phosphorylation, and destruction of microtubules and spines. *Journal of Neuroscience*, *30*, 11938–11950.

Zhao, J., Blayney, A., Liu, X., Gandy, L., Jin, W., Yan, L., Ha, J. H., Canning, A. J., Connelly, M., Yang, C., Liu, X., Xiao, Y., Cosgrove, M. S., Solmaz, S. R., Zhang, Y., Ban, D., Chen, J., Loh, S. N., & Wang, C. (2021). EGCG binds intrinsically disordered N-terminal domain of p53 and disrupts p53-MDM2 interaction. *Nature Communications*, *12*, 986.

Zhou, L., McInnes, J., Wierda, K., Holt, M., Herrmann, A. G., Jackson, R. J., Wang, Y. C., Swerts, J., Beyens, J., Miskiewicz, K., Vilain, S., Dewachter, I., Moechars, D., de Strooper, B., Spires-Jones, T. L., de Wit, J., & Verstreken, P. (2017). Tau association with synaptic vesicles causes presynaptic dysfunction. *Nature Communications*, *8*, 15295.

Zhu, Q. Y., Zhang, A., Tsang, D., Huang, Y., & Chen, Z. Y. (1997). Stability of green tea catechins. *Journal of Agricultural and Food Chemistry*, *45*(12), 462–446.

SUPPORTING INFORMATION

Additional supporting information can be found online in the Supporting Information section at the end of this article.